Science of the Total Environment 800 (2021) 149486

Contents lists available at ScienceDirect

Science of the Total Environment

journal homepage: www.elsevier.com/locate/scitotenv

Geochemistry and oxidative potential of the respirable fraction of powdered mined Chinese coals

Pedro Trechera [a,b], Teresa Moreno [a], Patricia Córdoba [a], Natalia Moreno [a], Fulvio Amato [a], Joaquim Cortés [a], Xinguo Zhuang [c], Baoqing Li [c], Jing Li [c], Yunfei Shangguan [c], Ana Oliete Dominguez [d], Frank Kelly [d], Takoua Mhadhbi [e], Jean Luc Jaffrezo [e], Gaelle Uzu [e], Xavier Querol [a,c,*]

[a] Institute of Environmental Assessment and Water Research (IDAEA), Spanish Research Council (CSIC), 08034 Barcelona, Spain
[b] Department of Natural Resources and Environment, Industrial and TIC Engineering (EMIT-UPC), 08242 Manresa, Spain
[c] Key Laboratory of Tectonics and Petroleum Resources, China University of Geosciences, Ministry of Education, Wuhan 430074, China
[d] MRC-PHE Centre for Environment and Health, King's College London, London SE1 9NH, UK
[e] Univ. Grenoble Alpes, IRD, CNRS, Grenoble INP, IGE (UMR 5001), 38000 Grenoble, France

HIGHLIGHTS

- Mo, Mn, Hf and Ge decrease in respirable fractions and Cs, W, Zn and Zr increase.
- AA is associated with inorganic matter, GSH and DTT with organic matter.
- OP^{AA} was clearly linked with Fe ($r = 0.83$) and pyrite ($r = 0.66$).
- OP^{GSH} was associated with moisture ($r = 0.73$), Na ($r = 0.56$) and B ($r = 0.51$).
- OP^{DTT} was highly correlated with Mg ($r = 0.70$), Na ($r = 0.59$) and B ($r = 0.47$).

GRAPHICAL ABSTRACT

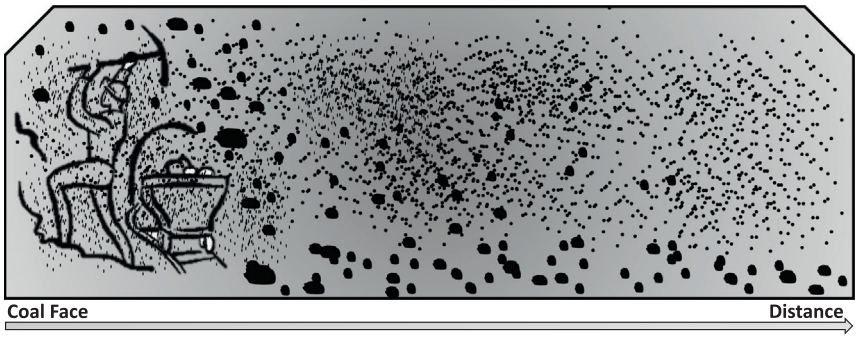

ARTICLE INFO

Article history:
Received 17 June 2021
Received in revised form 29 July 2021
Accepted 2 August 2021
Available online 5 August 2021

Editor: Pavlos Kassomenos

Keywords:
Chinese coal
Respirable dust
Oxidative potential
Coal dust
Coal geochemistry

ABSTRACT

This study evaluates geochemical and oxidative potential (OP) properties of the respirable (finer than 4 μm) fractions of 22 powdered coal samples from channel profiles (CP_4) in Chinese mined coals. The CP_4 fractions extracted from milled samples of 22 different coals were mineralogically and geochemically analysed and the relationships with the OP evaluated. The evaluation between CP_4/CP demonstrated that CP_4 increased concentrations of anatase, Cs, W, Zn and Zr, whereas sulphates, Fe, S, Mo, Mn, Hf and Ge decreased their CP_4 concentrations. OP results from ascorbic acid (AA), glutathione (GSH) and dithiothreitol (DTT) tests evidenced a clear link between specific inorganic components of CP_4 with OP^{AA} and the organic fraction of OP^{GSH} and OP^{DTT}. Correlation analyses were performed for OP indicators and the geochemical patterns of CP_4. These were compared with respirable dust samples from prior studies. They indicate that Fe ($r = 0.83$), pyrite ($r = 0.66$) and sulphate minerals ($r = 0.42$) (tracing acidic species from pyrite oxidation), followed by S ($r = 0.50$) and ash yield ($r = 0.46$), and, to a much lesser extent, Ti, anatase, U, Mo, V and Pb, are clearly linked with OP^{AA}. Moreover, OP^{GSH} correlation was identified by organic matter, as moisture ($r = 0.73$), Na ($r = 0.56$) and B ($r = 0.51$), and to a lesser extent by the coarse particle size, Ca and carbonate minerals. In addition, Mg ($r = 0.70$), B ($r = 0.47$), Na ($r = 0.59$), Mn, Ba, quartz, particle size and Sr regulate OP^{DTT} correlations. These became more noticeable when the analysis was done for samples of the same type of coal rank, in this case, bituminous.

* Corresponding author at: Institute of Environmental Assessment and Water Research (IDAEA), Spanish Research Council (CSIC), 08034 Barcelona, Spain.
E-mail addresses: xavier.querol@idaea.csic.es (X. Querol), pedro.trechera@idaea.csic.es (P. Trechera).

https://doi.org/10.1016/j.scitotenv.2021.149486

1. Introduction

1.1. Chinese coal and coal geochemistry

The use of coal in Chinese society can be traced back, with references to coal mining 3490 years ago (Dodson et al., 2014). Early documents refer to the use of Chinese coal for heating, cooking and smelting steel dating from 300 BCE (Gelegdorj et al., 2007; Li and Lu, 1995).

Nowadays, China is the greatest worldwide coal producer and consumer, with over half of the world's total consumption (BP, 2020; IEA, 2020; WCA, 2020). This situation will remain unchanged over the next few decades (Fan and Xia, 2012; Li et al., 2017; Wang et al., 2011; Yang et al., 2016).

Therefore, coal is the main source of energy production, representing 70% of the primary energy supply in China (Jie et al., 2020; J. Li et al., 2019; Qiao et al., 2019; Yuan, 2018). Some Chinese industrial sectors are directly dependent on coal for producing raw materials, such as steel, glass, cement or fertilizers (Lin and Tan, 2017; Wei et al., 2020).

China's coal resources have reached 13% of the global share (142 billion tonnes, BP, 2020), which account for 92–94% of the Chinese fossil fuel resources (Han et al., 2018; J. Li et al., 2019; Mao and Tong, 2013). Therefore, the large amount of coal production also requires large numbers of workers, which in China is around 5.5 million coal miners, according to Chen et al. (2013). Coal resources are widespread across China, where a prevalence of high rank over low rank coals (11% anthracite, 6% semi-anthracite, 70% bituminous coal, and 13% sub-bituminous coal and lignite) have been noticed (Mao and Tong, 2013). In these resources, a wide range of coal qualities from a large variety of coal basins in different geochemical regions are found, also accompanied by geochemical anomalies. Thus, Chinese coal ranges from the high-quality enormous coal resources from the Xinjiang Province (Li et al., 2012, 2014; Zhuang et al., 2012) to coals that contain such a high content of metals that they can be considered a source for these metals (Dai et al., 2003, 2016).

Examples of geochemical anomalies in coals from Northern China include high enrichment in Mn, Mg, Bi, Be, Cd, Mo, REEs and Y in the Huainan coalfields (Munir et al., 2018). There is a considerable content of Li and Ga in coals from the Jungar Coalfield, Inner Mongolia (Dai et al., 2012; J. Li et al., 2016). An elevated concentration of Zn, Pb and Cr can be found in coals from Yuyang, Hengshan, Shenmu, Huangling and Lingwu regions (Wang et al., 2014). Coals high in Mn, Nb and Ta have been extracted from the Jimunai depression (B. Li et al., 2019a). Coals with elevated concentration of REEs, Y, Nb, Ta, Zr, Hf, Ga, Th, and U have originated from the Qiandongbei coalfield (B. Li et al., 2020). The Gemudi mine contains coals with higher levels of V (Du et al., 2021) and coals with greater levels of As have been located in Southwestern China (Guo et al., 2017). Additionally high As, Ge, and U coals have been found in Shengli (Liu et al., 2021; Zhuang et al., 2006). This list of anomalies is not comprehensive (Dai et al., 2003, 2016; Tian et al., 2013; Yuzhuang et al., 2015).

Furthermore, some mineralogical enrichments have also been described for specific Chinese coals. In the Yueliangtian coal mining district, in Southwestern China, Wang et al. (2016) reported elevated concentrations of quartz in coal, due to precipitated siliceous solutions from the weathering of the Emeishan basalt. In northern China, Dai et al. (2010) reported high pyrite contents in #12 coal in the Songzao Coalfield, originating from a synsedimentary marine transgression over peat deposits and high Fe derived mainly from the mafic tuffs.

1.2. Coal geochemistry and mining occupational health

The high geochemical anomalies in coals in relation to some strategic elements such as Li, Ga or REEs, are very relevant from the point of view of their potential benefits (Qin et al., 2015; Zhang et al., 2015, 2020) but, in some cases, these might also be relevant from environmental and occupational points of view. Environmentally potentially hazardous elements can be directly emitted during coal use, extraction or transport of coal, the disposal of coal mining wastes and coal combustion by-products (Izquierdo and Querol, 2012).

High coal dust exposure levels is a matter of concern as may increase the occupational health risk (Landen et al., 2011; Liu et al., 2020; Masto et al., 2017; Zazouli et al., 2021) according to specific geochemical anomalies of coals (Fan and Xu, 2021; Liu and Liu, 2020; Moreno et al., 2019). There are several occupational diseases known to derive from coal handling, including lung diseases caused by excessive respirable crystalline silica (RCS). Intensive research has been carried out on the occupational health impacts of coal dust associated with coal workers' pneumoconiosis (CWP), silicosis and the possibility of pulmonary fibrosis (Mo et al., 2014; NIOSH, 2002). Specific studies concluded that "quartz is not the predominant factor in the development of CWP" (McCunney et al., 2009); and others have implicated transition metals, such as bioavailable Fe or Ni, as relevant contributors to the development of CWP (Christian et al., 1979; Harrington et al., 2012; Huang et al., 2002, 2005; McCunney et al., 2009).

Although, CWP is one of the most common disease in occupational coal mining, other pathologies can be linked to high levels of coal dust exposure (Ávila Júnior et al., 2009; Pedroso-Fidelis et al., 2020; Wilhelm Filho et al., 2010; Yu et al., 2020, among others). Nardi et al. (2018) indicated that inflammatory and oxidative stress parameters are potential early biomarkers for silicosis.

Frequent exposure to respirable pyrite particles in coal dust over time promotes a chronic level of inflammation, developing hydrogen peroxide and ferrous Fe, which produce highly reactive hydroxyl radicals, contributing to the pathogenesis of CWP (Cohn et al., 2006b; Harrington et al., 2012). Furthermore, several studies link pyrite contents in coal and coal dust with reactive oxygen species (ROS) generation, ROS in cells and a potential role in the pathogenesis of CWP (Castranova, 2000; Cohn et al., 2006a; Harrington et al., 2012; Huang and Finkelman, 2008; Liu and Liu, 2020; Moreno et al., 2019; Murphy and Strongin, 2009; Zosky et al., 2021).

In coal, sulphate can occur naturally or also through the oxidation of sulphide minerals during mining (Wang et al., 2017). Liu and Liu (2020) evidenced that sulphate nanoparticles exist in the mining environment, which can cause depression of pulmonary particle clearance and asthma due to the high biological activity.

There is considerable research on the production of ROS through increased concentrations of various metallic elements in dust, including Cu, V, Cr, Fe, Mn, Pt, Zn, Ni, Mo, Co, V and Pb (Cohn et al., 2006a; Fu et al., 2014; Huang et al., 2005; Latvala et al., 2016; Liu and Liu, 2020; Valko et al., 2005, among others). Moreover, Cr could be related to lung cancer in coal mine workers (WHO, 2000), and elevated exposure to Pb could be linked to the development of neurological toxins (Moreno et al., 2019). All in all, due to the widely different and heterogeneous compositions of coal, different diseases through exposure to coal mining and handling can potentially be developed by coal workers. Finkelman et al. (2002) gave an overview of possible health effects of coal and coal use.

Another risk associated with coal dust is its impact on ecological and environmental pollution, affecting communities in areas surrounding coal mining activities (Ishtiaq et al., 2018; Lashgari and Kecojevic, 2016; Masto et al., 2017; Tang et al., 2017). Moreover, high underground coal dust concentrations may lead to spontaneous combustion (Li et al., 2021; Liu et al., 2020; Ma et al., 2020; Querol et al., 2011; Shimura and Matsuo, 2019).

This study aims to evaluate the relationships between a variety of coal geochemical and mineralogical anomalies in a wide variety of mined Chinese coals with oxidative potential (OP), focusing on the respirable coal dust fraction (occupational exposure), by extracting and characterising the respirable fractions of the selected powdered coal samples. Respirable dust is the mass fraction of inhaled particles that are able to penetrate the respiratory tract and reach the non-ciliated, gas exchange, alveolar region of the lung. This fraction is attributed to

coal dust particles <4 μm mass median diameter (D_{50} = 4 μm) (Brown et al., 2013; European Committee for Standardization, 1992; Sánchez Jiménez et al., 2011).

To validate the method used, the analyses were repeated by including more results, namely those obtained by Trechera et al. (2020, 2021) on recently coal mine dust samples.

2. Methodology

2.1. Selection of coal samples: geological and geochemical settings

Twenty coal channel profile (CP) samples from six Chinese provinces were selected in this study (Fig. 1). These include fifteen underground coal mines, one open-pit coal mine and two coal exploration boreholes. Additionally, two Vietnamese coal samples (CP_21 and CP_22, not included in Fig. 1), were also selected. This selection was based on geochemically anomalous coals previously studied by the authors and sample availability. The reasons for sample selection and a brief description of their origin are summarised below:

- CP_01 and CP_02 were collected from underground coalfaces of the #11 and #5 coals, respectively, from the Sangshuping coal mine (Southeastern Shaanxi Province). These Late Carboniferous (Taiyuan Formation) coals have different geochemical patterns and coal rank (#11 is a low-volatile, LV, bituminous according to ASTM D388-12 and #5 coal a semi-anthracite). The first is a high organic S coal, with relatively low pyrite content, while the second is a low S and middle ash yield coal (J. Li et al., 2020).
- CP_03 was collected from underground coalfaces of the #5 coal from the Yongming coal mine (Northern Shaanxi Province). This is a Late Triassic (Wayaobao Formation) high-volatile (HV) bituminous coal. This is a high Sr coal (authors' unpublished data).
- CP_04 and CP_05 were collected from the high-Ge Wulantuga open-pit coal mine in the Shengli Coalfield, Northeastern Inner Mongolia. This #6 coal seam, Early Cretaceous Shengli Formation, reaches the sub-bituminous coal rank. These are coals with high Ge, As and W contents (Li et al., 2011).
- CP_06 and CP_07 were collected from #6 coal seam from the Junggur Coalfield, in the Buertaohai-Tianjiashipan coal mining district (Inner Mongolia) in two exploration boreholes (Borehole ZK43-25 and ZK17-15, respectively). This is a Late Carboniferous (Taiyuan Formation) HV bituminous coal. The first was selected for its high Pb content, and the second for the slight enrichment in Th (J. Li et al., 2016).
- CP_08 coal was collected from the underground working face of #4 coal from the Chunlei coal mine (Northeastern Guizhou) working Late Permian (Wujiaping Formation) medium-volatile (MV)

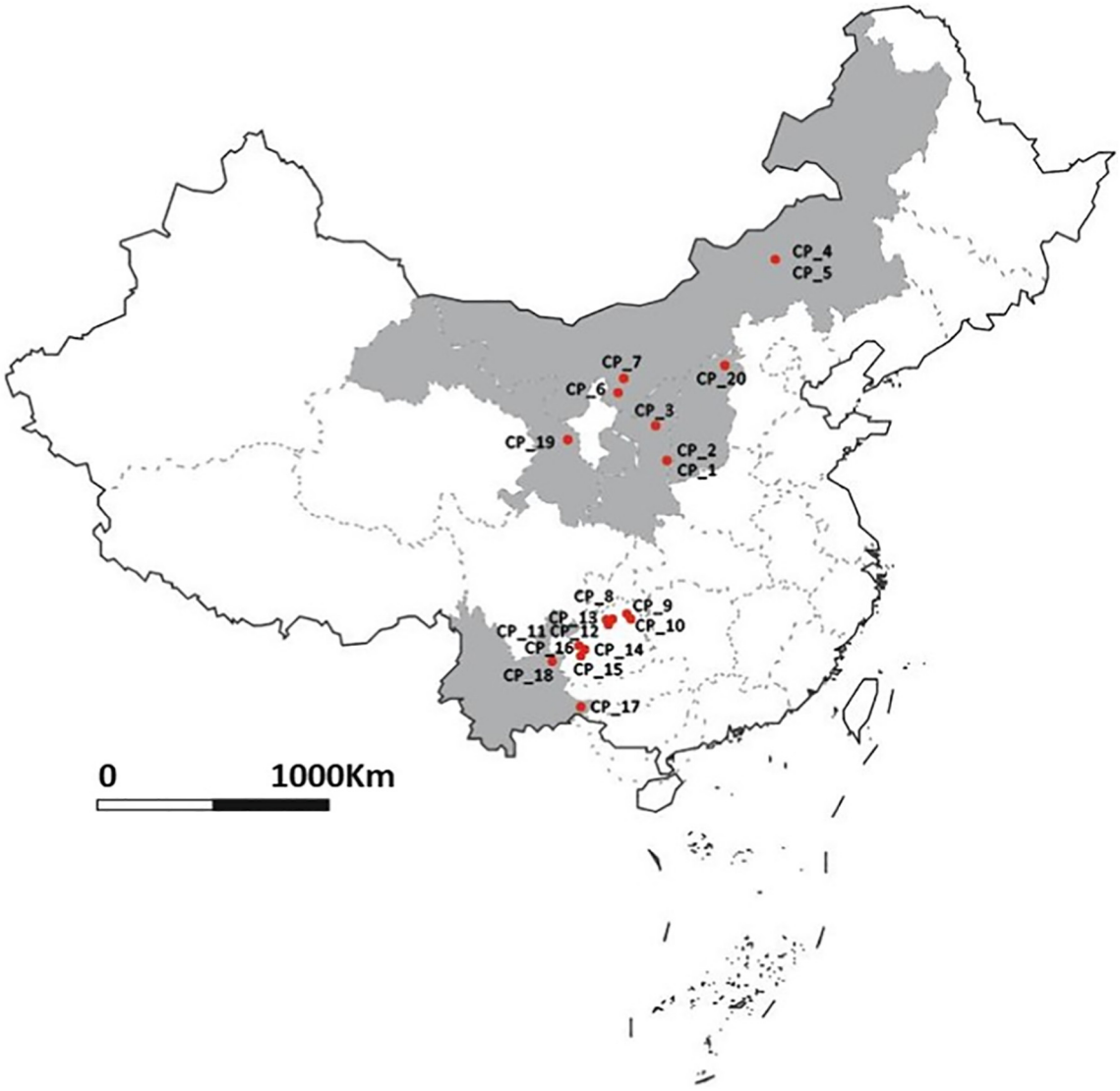

Fig. 1. Location of the 20 coal samples collected from different coal mines in China. Two Vietnamese coal samples, CP_21 and CP_22, not included in the figure.

bituminous coals. This coal has a high ash yield, pyrite and metals (Zn, Zr, REEs, Y, Nb, Pb, Cd, Ni, Cr, As, Se) (B. Li et al., 2019b).

- CP_09 and CP_10 were also obtained from the Late Permian (Wujiaping Formation) coals but, in this case, from the Jinqi and Yudai underground mines in the Qiandongbei Coalfield (Northeastern Guizhou), working MV and LV bituminous coals, respectively. Geochemically these are very different coals. The first is a high ash yield, pyrite and metals (V, Mo, Cr, U, As) coal, while the second is also a high pyrite coal but enriched in other metals (Pb, As, Se, Y, Nb, REEs) (B. Li et al., 2020).
- CP_11 and CP_12 were also collected from the Late Permian (Wujiaping Formation); in this case, from the underground working face of the LV bituminous C4 coal from the Chalinbao coal mine in the Tongzi Coalfield (Northeastern Guizhou). The first is a high Sr middle ash yield coal, and the second a high P and very high Sr coal (B. Li et al., 2019b).
- CP_13 was collected from C2 coal seam in Tiedingyan underground coal mine (Northeastern Guizhou), mining also Late Permian (Wujiaping Formation) LV bituminous coal. This is a very high Ti coal with moderate enrichments in Th, Y, Zr and REE (authors' unpublished data).
- CP_14 and CP_16 were obtained from the Late Permian (Longtan Formation) anthracite coals in the Fenghuangshan and Wenjiaba underground coal mines of the China Coalfield (Western Guizhou). The first is a middle ash yield and S coal enriched in Mo, V and U, and the second a middle ash yield coal enriched in Li (Li et al., 2017).
- CP_15 was obtained from the Late Permian (Longtan Formation) LV bituminous coal, worked in the Liulong underground mine of the Liuzhi coalfield (Guizhou Province). This is a High Sr and Mn coal (B. Li et al., 2016).
- CP_17 was collected from the Puyang underground coal mine (Southeastern Yunnan), working Tertiary (Xiaolongtan Formation) lignite. This is a high ash yield, moderately enriched in aluminium-silicate associated metals (Cr, Rb, Cu and Ni) (authors' unpublished data).
- CP_18 was collected from the Quqing underground coal mine (Eastern Yunnan), working Late Permian (Longtan Formation) HV bituminous coals. This is a high carbonate minerals coal enriched in Sr and Mn (authors' unpublished data).
- CP_19 was taken from the Wangjiashan underground coal mine (Central Gansu), working Jurassic (Yaojie Formation) HV bituminous coal. This is a low ash yield coal, moderately enriched in B (authors' unpublished data).
- CP_20 was obtained from the HV bituminous Early Permian coal worked (Shanxi Formation) in the Datong coal mine (Shaanxi province). This is a low ash yield and high Sr coal (authors' unpublished data).
- CP_21 and CP_22 were obtained from the Nui Houg Late Triassic coal mine, in Thai Nguyen Province of Vietnam. These coals are highly enriched in As, Mo, Sb, U and Tl (authors' unpublished data).

2.2. Sample treatment and analyses

In order to obtain a precise representation of the coal seam, the samples were collected using the CP approach, vertically across the coal seams, and stored in plastic bags to avoid oxidation. Samples were first analysed for bulk mineralogical and geochemical characterisation of the parent coal. Subsequently, a riffled fraction of the sample was milled using the same automatic agate mortar and time, and the resulting powdered coal sub-samples used to extract the respirable fraction (<4 μm, CP_4). Afterwards, a complete particle size distribution (PSD), mineralogical and geochemical characterisation was obtained from each CP_4. In parallel, OP analyses were also performed for each CP_4 with the aim of evaluating links between geochemical patterns and ROS. Finally, this link was evaluated again including data from recently coal mine dust collected (Trechera et al., 2020, 2021). This was performed in order to validate the results obtained using the laboratory protocol explained in this study to obtain samples representing respirable coal dust from powdered coal samples.

2.2.1. Sample pre-treatment

In order to separate the respirable fraction of coal powder samples, a special chamber resuspension device was used, due to the small amount of powdered sample available. Furthermore, the efficiency of technique was tested before analysis, using different coal ranks, changing the filter collector and optimising the best flow-rates.

A total of twenty-two coal samples (twelve bituminous, five semi-anthracites, three sub-bituminous/lignite and two anthracite) were analysed. First, 5.0 g of each sample were milled with a Mortar Agatha Grinder RM 200 in an automatic mode for exactly 2 min. Second, using a mobile chamber resuspension device separator, the CP_4 fraction was obtained from a riffled sub-sample of each powdered coal using a laboratory particulate matter (PM), PM_{10}-$PM_{2.5}$ powdered dust sampler (Moreno et al., 2008). Briefly, the coal powder was spread onto a glass tray surface and, with the corresponding vacuum (30 $L \cdot min^{-1}$ of airflow), the sample was suctioned into a methacrylate chamber. The sample was advanced through a <4 μm inlet and finally the CP_4 sample was deposited on the surface of a polycarbonate filter with 47 mm diameter and 0.6 size porosity. The size cut off depends on the flow, therefore experiments were carried out to find the optimal flow for <4 μm. The sample deposited into a methacrylate chamber was recollected, spread onto a glass tray surface again and repeated the CP_4 separation procedure. Finally, the sample collected, around 300–400 mg, on the filter surface was brushed prudently and ready for the subsequent analysis.

2.2.2. Dry particle size distribution

With the aim to confirm that the respirable fraction was separated from the powdered CP sample, Malvern Scirocco 2000 analyses were performed for each CP_4 sample.

A Malvern Mastersizer, coupled to a Scirocco 2000 extension, was used to analyse the dry PSD and confirm that the median particle diameter (D_{50}) of each CP_4 was close to 4 μm as required to be 'respirable'. Furthermore, for each CP_4 sample D_{10}, D_{25} and D_{75} values were obtained for evaluating the potential links between PSD and OP for CP_4 samples.

2.2.3. Mineralogical analysis

In order to analyse the mineralogical characterisation of parent bulk coal and the respective CP_4 samples, a powder X-ray diffraction (XRD) was used with A Bruker D8 Advance A25, θ-θ diffractometer with CuKα1 radiation, Bragg-Brentano geometry, and a position-sensitive Lynx Eye detector. Diffractograms at 40 kV and 40 mA, scanning from 4 to 60° of 2 θ with a step size of 0.019° and a counting time of 0.10 $s \cdot step^{-1}$ maintaining the sample in rotation (15 min) were performed. The crystalline phase identification was conducted using the EVA software package (Bruker), which utilised the ICDD (International Centre for Diffraction Data) database. Semi-quantitative XRD analysis was performed using the method devised by Chung (1974) for the quantitative analysis of multi-component systems, using quartz as an internal reference. Chung's method was used on mixtures, which were obtained from powdered mineral reference materials and coal with low ash to validate the semi-quantitative protocol, shown in Fig. S1.

2.2.4. Proximate, ultimate and chemical analyses

In order to evaluate the composition of CP and CP_4 several geochemical analyses were performed. Proximate and ultimate analyses followed ISO and ASTM procedures (ISO-589, 1981, ISO-1171, 1976, ISO-562, 1974, ASTM D-3286, D-3302M, D3174-12), with moisture and ash yield obtained at 150 °C and 750 °C, respectively.

Before major and trace element analyses, 0.10 g of samples of the parent coal and CP_4 samples were digested in HF-HNO_3-$HClO_4$ acid following the method by Querol et al. (1992, 1997) to retain potentially volatile elements, such as As and Se. The resulting acidic digestions were analysed for major and trace elements by using inductively-coupled plasma atomic-emission spectrometry (ICP-AES, Iris Advantage Radial ER/S device from Thermo Jarrell-Ash) and inductively-coupled plasma mass spectrometry (ICP-MS, X-SERIES II Thermo Fisher

Scientific, Bremen, Germany). International reference materials SARM19 and NIST SRM 1633b, and blanks were treated in the same way.

Using the same analytical approaches and type for coal and coal mine dust samples (Trechera et al., 2020, 2021), adding two more repetitions, elements analysed reported the analytical errors shown in Table S1.

Because Si is lost during HF digestion, its contents in coal samples and CP_4 were determined by X-ray fluorescence (XRF, Thermo Scientific ARL QUANT'X Energy-Dispersive X-ray fluorescence spectrometer) loading Teflon© 47 mm filters with 3.0 mg of the sample using an ethanol suspension. This method was validated using the above reference materials.

2.2.5. Oxidative potential

In order to evaluate the links between geochemical patterns of CP_4 and oxidative stress, an OP test was performed for each sample. OP is an indicator of the capacity to generate ROS in human bodies that may result in oxidative stress. Several studies have linked respiratory disorders and lung diseases to the ROS formation in cells (Imai et al., 2008; Kelly, 2003; Kim et al., 2018; Pietrogrande et al., 2021; Rahman and Adcock, 2006). In addition, oxidative stress plays a key role in understanding how atmospheric suspended PM affects health through respiratory inflammation, lung cancer, and chronic cardiopulmonary diseases, among others (Fang et al., 2019; Janssen et al., 2014; Kelly, 2003; Leni et al., 2020; MacNee, 2001; Y.J. Zhang et al., 2021).

The oxidative stress of the CP_4 samples was evaluated via the OP method in two different laboratories. Firstly, OP method was performed in King's College of London, which is based on the consumption of ascorbic acid (AA), urate (UA) and glutathione (GSH) antioxidants, as described in detail by Soltani et al. (2018). The OP analysis involves the resuspension of each CP_4 sample in ethanol and a 4 h incubation with a synthetic solution containing equi-molar concentrations of antioxidants. The consumption of these antioxidants is determined following the methodology by Baker et al. (1990) and Iriyama et al. (1984). In-house controls of PM-free, negative PM (M120, Cabot Corporation, USA) and positive PM (NIST1648a, urban particulate from NIST, USA) followed the same protocol for control purposes.

Secondly, OP analyses were also carried out in Grenoble Alpes University, this time based on the consumption of dithiothreitol (DTT) antioxidants, as described in detail by Calas et al. (2018). For each sample, 40 μL of PM suspension (in triplicate) with 205 μL of phosphate buffer (pH = 7.4) were incubated at 37 °C in 12.5 nmol of DTT (DTT solution in phosphate buffer). Reaction was stopped at 0, 15 and 30 min adding 50 nmol of 5,5′-dithiobis (2-nitrobenzoic acid) (DTNB in phosphate buffer). A solution of 40 μL of 1,4 naphtoquinone (1,4-NQ 24.7 μM) was used as positive control. DTT consumption by formation of DTT-disulfide form in presence of ROS (Yang et al., 2014) was measured at 412 nm using a plate-reader TECAN spectrophotometer Infinite® M 200 pro and 96 well CELLSTAR® plates. OP was obtained from the slope of the linear regression of the consumed DTT (corrected from blank measurements and from matrix absorbance from particles) normalized by the PM_{10} mass (nmol DTT min^{-1} μg^{-1}).

The OP of the CP_4 samples was expressed as the percentage of consumption of each antioxidant with reference to the in-house, particle-free control. To obtain a metric for the OP, the data were expressed as OP per μg ($OP^{AA}\mu g^{-1}$, $OP^{GSH}\mu g^{-1}$, $OP^{DTT}\mu g^{-1}$). Since AA and GSH were mixed in the same assay, individual antioxidant depletions were also combined to provide a total OP value (OP^{TOTAL}(OP^{AA+GSH}) μg^{-1}).

2.2.6. Data analysis

Data obtained from the PSD, mineralogical and geochemical characterisations were evaluated for correlation with OP patterns by using the software StataCorp LLC (College Station, Texas, USA) version Stata/SE 15.1.

2.3. Limitations of the methodology used

The present study was carried out through the selection of coal samples (CP), milling the samples and obtaining the respirable fraction (<4 μm) of each CP sample (CP_4). In addition, the subsequent evaluation took place under similar conditions (atmospheric particulate matter finer than 4 μm, PM_4) present in the coal mine from where the CP sample was collected. The conditions could not be fully replicated because, in the coal mine, sources of PM include not only the dust from the worked coal seam, but also from the other sediments where coal is interlayered, wear of machinery, salts and other components from precipitates of acidic mine drainage, among others (Trechera et al., 2020).

Furthermore, when working the coal seam, coal can be powdered in a very different way to a laboratory mill, with some coal components being enriched or depleted in the respirable fractions. However, collecting respirable dust samples in the numerous Chinese mines included in this study, would have required considerably more time and increased costs. Furthermore, the objective of this study is to analyse the geochemical patterns of coal that might enrich a given coal dust in specific elements and minerals and to evaluate the effect of these enrichments on OP of dust. Thus, it was considered that, in spite of the above limitations, this method is useful for the aims of this study.

To support this, at the end of the manuscript the results of the joint evaluation of OP and geochemical patterns for a compiled set of true respirable dust obtained from deposited coal mines, together with the 22 CP_4 samples is presented. If associations of elements, minerals and coal patterns with OP remain unchanged with respect to the single analysis of the CP_4 sets, this will support the applicability of the method.

3. Results and discussion

3.1. Mineralogy and geochemistry

Results from proximate and ultimate analyses of the coal samples are shown in Table 1, while Tables 2 and 3 illustrate mineral and elemental concentrations from all parent coal samples analysed in this study. Tables 4 and 5, following, show the same data for CP_4 samples.

3.1.1. Parent coals

Tables 1 and 2 show that samples CP_08, CP_09 and CP_17 (bituminous the first two and lignite the last) have a high mineral matter content, with ash yields of 32, 34, and 34% dry basis (db), respectively. Sample CP_17 contains a high quartz content (15% weight, % wt), and CP_08, CP_14 and CP_09 are high pyrite coals (6, 5 and 14% wt, respectively). Furthermore, CP_08 has a high carbonate minerals content (3 and 11% wt, ankerite and calcite, respectively,) as does CP_18 (1 and 12% wt, ankerite and calcite); while CP_09 and CP_10 contain a relatively high sulphate minerals content (4–5% wt), CP_21 high tobelite (13% wt, an illitic clay with NH_4^+ replacing K^+).

The major and trace element contents of the bulk CP parent coals were compared with their respective Chinese average concentrations, Table S2 (Dai et al., 2007, 2008) to evidence specific geochemical enrichments. The most relevant geochemical enrichments for each sample are summarised in Table 6, in comparison with Chinese geochemical averaged concentrations.

3.1.2. Geochemistry of the <4 μm fraction of the powdered coals

Fig. S2 and Table S3 show the PSD of CP_4 samples, with the percentiles of the diameter, and evidence the efficiency of the separation technique and procedure conducted during the analysis, because D_{50} of CP_4 are in all classes remarkably close to 4.0 μm.

Fig. 2 shows the average ratios of the mineral contents between the CP_4 samples and the respective bulk powdered parent coal (CP_4/CP). As expected, high similarities between CP_4 and CP mineralogy were found, with average ratios close to 1. However, several exceptions were detected, such as sulphate minerals, slightly depleted in CP_4 (ratios close

Table 1
Details of the origin of all coal channel profiles (CP) collected in mines across China for this study and data from proximate analysis. M, Moisture; ad, air dry; db, dry basis; VM, Volatile Matter; LV, Low-Volatile; HV, High-Volatile; MV, Medium-Volatile.

Sample	M (%ad)	Ash (%db)	VM (%)	Rank	Sampling location	Province	Geological age
CP_01	0.25	9.36	15.40	LV bituminous	Sangshuping Coal mine	Shaanxi Province, Southeastern China	Late Carboniferous, Taiyuan Formation
CP_02	0.19	7.97	13.70	Semi-anthracite	Sangshuping Coal mine	Shaanxi Province, Shoutheastern China	Late Carboniferous, Taiyuan Formation
CP_03	1.20	21.31	41.50	HV bituminous	Yongming Coal mine	Shaanxi Province, northwest China	Late Triassic, Wayaobao Formation
CP_04	8.31	7.51	51.20	Sub-bituminous	Wulantuga Coal mine	Inner Mongolia, northeastern China	Early Cretaceous, Shengli Formation
CP_05	9.73	9.39	46.12	Sub-bituminous	Wulantuga Coal mine	Inner Mongolia, northeastern China	Early Cretaceous, Shengli Formation
CP_06	2.51	16.74	36.80	HV bituminous	Junggur Coalfield Borehole	Inner Mongolia, northeastern China	Late Carboniferous, Taiyuan Formation
CP_07	4.16	16.05	37.50	HV bituminous	Junggur Coalfield Borehole	Inner Mongolia, northeastern China	Late Carboniferous, Taiyuan Formation
CP_08	0.99	32.33	26.84	MV bituminous	Chunlei Coal mine	Northeastern Guizhou Province, southwest China	Late Permian, Wujiaping Formation
CP_09	1.79	34.41	33.64	MV bituminous	Jinqi Coal mine	Northeastern Guizhou Province, southwest China	Late Permian, Wujiaping Formation
CP_10	2.95	22.48	21.46	LV bituminous	Yudai Coal mine	Northeastern Guizhou Province, southwest China	Late Permian, Wujiaping Formation
CP_11	0.49	10.81	13.80	Semi-anthracite	Chalinbao Coal mine	Northeastern Guizhou Province, southwest China	Late Permian, Wujiaping Formation
CP_12	0.49	17.28	14.65	Semi-anthracite	Chalinbao Coal mine	Northeastern Guizhou Province, southwest China	Late Permian, Wujiaping Formation
CP_13	0.49	22.98	20.99	LV bituminous	Tiedingyan Coal mine	Northeastern Guizhou Province, southwest China	Late Permian, Wujiaping Formation
CP_14	1.59	14.81	7.87	Anthracite	Fenghuangshan Coal mine	Western Guizhou Province, southwest China	Late Permian, Longtan Formation
CP_15	0.91	18.39	20.11	LV bituminous	Liulong Coal mine	Western Guizhou Province, southwest China	Late Permian, Longtan Formation
CP_16	1.29	10.65	7.45	Anthracite	Wenjiaba Coal mine	Western Guizhou Province, southwest China	Late Permian, Longtan Formation
CP_17	7.05	34.25	60.70	Lignite	Puyang Coal mine	Southeastern Yunnan Province, southwest China	Tertiary, Xiaolongtan Formation
CP_18	2.00	14.09	39.30	HV bituminous	Quqing Coal mine	Eastern Yunnan Province, southwest China	Late Permian, Longtan Formation
CP_19	7.47	2.76	37.90	HV bituminous	Wangjiashan Coal mine	Gansu Province, northwest China	Jurassic, Yaojie Formation
CP_20	8.28	4.51	39.40	HV bituminous	Datong Coal mine	Shaanxi Province, north China	Early Permian, Shanxi Formation
CP_21	1.06	20.17	8.19	Semi-anthracite	Nui Houg Coal mine	Thai Nguyen Province, Vietnam	Late Triassic
CP_22	1.55	11.70	8.75	Semi-anthracite	Nui Houg Coal mine	Thai Nguyen Province, Vietnam	Late Triassic

to 0.8, melanterite mineral being almost completely absent in CP_4 fractions), and anatase, with a marked increase in CP_4 (×2.7) in most samples. Sulphate minerals in coal and coal dust occur usually in large crystals, commonly much larger than the respirable particle size, while anatase occurs generally as exceptionally fine crystal aggregates dispersed in both the organic and clay matrixes (Figs. 4 and S4 of Trechera et al. (2020, 2021), respectively).

Sulphate CP_4/CP ratios are positively correlated ($r = 0.74$) with moisture (% air dried, ad). Moisture potentially accelerates the process of oxidation of sulphides in coals (Allardice et al., 2003; Choi et al., 2011; Wang et al., 2003), which usually have a relatively fine PSD. Moreover, the adsorption of moisture can soften and lubricate the microstructures, weakening mechanical coal matrix properties (Ahamed et al., 2019; Ren et al., 2021). The highest CP_4/CP for sulphate minerals is obtained for sub-bituminous coals, probably induced by a higher moisture content, which causes more intense oxidation. On the other hand, carbonate minerals (especially calcite), ratios are correlated with the volatile matter (% dry ash free, daf), thus increasing towards low rank coals ($r = 0.74$ and 0.90 respectively) pointing to a finer size of calcite in lower coal rank coals. In fact, the ratios followed this trend HV > MV > LV (from 1.7 to 0.2) in bituminous coal. This is probably due to the recrystallisation processes, which are more probable in higher rank coals.

Average CP_4/CP for major elements (Fig. 2) reach 0.7 and 0.8 for Fe and S; while the P, Al and Na averaged ratios reach 1.2, 1.3 and 1.5, respectively. No correlations were observed between CP_4/CP of major elements and coal rank when including all coals, but $r = 0.87$ and -0.70 are reached for Fe and K ratios and moisture when only bituminous coals are evaluated. Thus, and accordingly, volatile matter is marginally correlated with Fe ratios ($r = 0.70$) and noticeable negatively correlated with K ($r = -0.74$).

Furthermore, ash yields are negatively correlated with Fe ($r = -0.80$) and S ($r = -0.81$), ratios pointing that high ash yield coals contain coarser pyrite than low ash ones. In fact, ash yield is correlated with pyrite contents in bituminous samples ($r = 0.80$ for CP and $r = 0.71$ CP_4). Thus, higher pyrite coal might contain coarser pyrite. In contrast, in low pyrite coals, fine framboidal pyrite is the prevailing form of this mineral. Thus, the highest ratios are obtained for samples with pyrite content below the XRD detection limit (CP_4_19 and CP_4_20). In prior studies on Chinese and European bituminous coals, the concentrations of Fe and S also decreased in the respirable coal dust fraction compared with the parent bulk coal dust (Trechera et al., 2020, 2021).

Concerning the CP_4/CP ratios of trace elements, those for Mo, Mn, Hf and Ge are generally <1.0, ($n = 10, 21, 13, 18$, respectively), with only six samples with ratios slightly >1.0 (four in the case of Mn and two in the one of Ge). These results concur with those of Trechera et al. (2020, 2021), especially as far as Mn is concerned. On the other hand, elements such as Cs, W, Zn and Zr increase their concentration in CP_4. Usually Hf and Zr are associated with zircon (Zr-silicate) in coal (Swaine, 1990); however, in this study, it seems that Hf is particularly concentrated in the coarser zircon. Mo and Ge are usually associated with organic matter (yielding coarser particles), while Mn is usually associated with carbonate minerals (Swaine, 1990).

3.2. Oxidative potential

3.2.1. Oxidative potential of the <4 μm fraction of the powdered coal samples (CP_4)

The OP test is defined as a measure of the capacity of PM to oxidise target molecules. The outputs of the OP are used as a predictor of biological responses to PM toxicity and might yield more information on the potential health effects than PM mass or chemistry (Ayres et al., 2008; Borm et al., 2007; Daellenbach et al., 2020). Although the OP analyses are not commonly used yet to characterise standard responses of coal dust, it could be a valuable technique to evaluate potential occupational hazards, since it integrates various biologically-relevant dust properties, including size, surface and mineralogical and chemical composition (Ayres et al., 2008; Janssen et al., 2014). Several methods for measuring OP are available, and agreement has not been reached on recommending one of them (Ayres et al., 2008; Calas et al., 2018; Moreno et al., 2017). Different tests monitor specific oxidative processes caused by particular PM or dust component types. Commonly, OP^{AA}, OP^{GSH}, and OP^{DTT} assays are used for PM exposure, based on the facts that AA and GSH are physiological antioxidants present in the lung and DTT is a strong reducing agent, chemical surrogates of antioxidants (Fang et al., 2017).

In these samples, OP^{TOT} average values reached 1.16 (0.4–2.0) $\%OP^{TOT}\mu g^{-1}$ ($OP^{TOT} = OP^{AA} + OP^{GSH}$, in % consumption·$\mu g^{-1}$) (Table 7). These OP values fall in the range reported for a number of Chinese actual

Table 2
Mineral contents (% wt) of the bulk coal channel profile samples (CP). Qtz, Quartz; Ant, Anatase; Cb, Carbonates; Py, Pyrite; Sul, Sulphates; Ill-Ms, Illite-Muscovite; Mm, Montmorillonite; Kln-Clc, Kaolinite-Clinochlore; Tob, Tobelite; Ank, Ankerite; Cal, Calcite; Dol, Dolomite; Sid, Siderite; Gy, Gypsum; Jar, Jarosite; Szo, Szomolnokite; Roz, Rozenite; Mel, Melanterite.

Sample	CP_01	CP_02	CP_03	CP_04	CP_05	CP_06	CP_07	CP_08	CP_09	CP_10	CP_11	CP_12	CP_13	CP_14	CP_15	CP_16	CP_17	CP_18	CP_19	CP_20	CP_21	CP_22
Clays	4.4	4.5	12.2	<dl	3.9	14.9	13.2	10.7	13.0	11.2	9.2	12.9	13.1	5.4	<dl	9.3	17.3	0.4	1.1	<dl	13.0	8.0
Qtz	<dl	<dl	5.1	3.6	3.8	<dl	1.2	0.6	2.8	0.7	<dl	<dl	<dl	2.3	4.7	<dl	15.4	<dl	0.3	4.5	4.9	3.0
Ant	<dl	<dl	<dl	<dl	<dl	<dl	<dl	<dl	<dl	<dl	<dl	<dl	<dl	0.7	0.6	0.5	<dl	<dl	<dl	<dl	0.3	0.2
Cb	4.1	3.4	3.6	<dl	<dl	0.4	1.5	14.5	<dl	<dl	<dl	0.4	9.6	<dl	6.2	<dl	<dl	13.5	1.3	<dl	<dl	<dl
Py	0.6	0.1	0.3	2.7	0.9	0.6	<dl	5.6	14.1	4.1	1.7	3.5	0.3	5.3	4.7	0.9	1.6	0.1	<dl	<dl	2.0	0.6
Sul	0.2	<dl	<dl	1.2	0.7	0.9	<dl	0.9	4.5	6.4	<dl	0.4	<dl	1.1	2.2	<dl	<dl	<dl	<dl	<dl	<dl	<dl
Ill-Ms	<dl	<dl	<dl	<dl	<dl	<dl	<dl	<dl	<dl	<dl	<dl	<dl	<dl	<dl	<dl	1.2	3.8	<dl	<dl	<dl	<dl	<dl
Mm	<dl	<dl	<dl	<dl	<dl	<dl	<dl	<dl	<dl	<dl	<dl	<dl	<dl	2.5	<dl	<dl	<dl	<dl	<dl	<dl	<dl	<dl
Kln-Clc	1.9	2.9	12.2	<dl	3.9	14.9	13.2	10.7	13.0	11.2	2.4	2.4	13.1	<dl	<dl	8.2	13.5	0.4	1.1	<dl	<dl	<dl
Tob	2.5	1.6	<dl	<dl	<dl	<dl	<dl	<dl	<dl	<dl	6.8	10.5	<dl	2.9	<dl	<dl	<dl	<dl	<dl	<dl	13.0	8.0
Ank	<dl	0.2	0.5	<dl	<dl	<dl	<dl	3.4	<dl	<dl	<dl	<dl	<dl	<dl	<dl	<dl	<dl	1.3	<dl	<dl	<dl	<dl
Cal	4.1	3.2	2.7	<dl	<dl	<dl	1.5	10.7	<dl	<dl	<dl	<dl	9.5	<dl	6.2	<dl	<dl	11.9	1.3	<dl	<dl	<dl
Dol	<dl	<dl	<dl	<dl	<dl	<dl	<dl	<dl	<dl	<dl	<dl	0.4	0.1	<dl	<dl	<dl	<dl	<dl	<dl	<dl	<dl	<dl
Sid	<dl	<dl	0.4	<dl	<dl	0.4	<dl	0.4	<dl	<dl	<dl	0.4	<dl	<dl	<dl	<dl	<dl	0.3	<dl	<dl	<dl	<dl
Gy	0.2	<dl	<dl	1.2	0.7	<dl	<dl	0.5	<dl	0.4	<dl	<dl	<dl	<dl	<dl	<dl	<dl	<dl	<dl	<dl	<dl	<dl
Jar	<dl	<dl	<dl	<dl	<dl	<dl	<dl	<dl	<dl	<dl	<dl	0.4	<dl	<dl	<dl	<dl	<dl	<dl	<dl	<dl	<dl	<dl
Szo	<dl	<dl	<dl	<dl	<dl	<dl	<dl	<dl	2.7	1.2	<dl	<dl	<dl	<dl	2.2	<dl	<dl	<dl	<dl	<dl	<dl	<dl
Roz	<dl	<dl	<dl	<dl	<dl	<dl	<dl	<dl	1.8	2.8	<dl	<dl	<dl	1.1	<dl	<dl	<dl	<dl	<dl	<dl	<dl	<dl
Mel	<dl	<dl	<dl	<dl	<dl	0.9	<dl	0.5	<dl	2.1	<dl	<dl	<dl	<dl	<dl	<dl	<dl	<dl	<dl	<dl	<dl	<dl

respirable coal mine dust samples by Trechera et al. (2020, 2021), with 0.3–0.8%$OP^{TOT}\cdot\mu g^{-1}$ for coal open-pit mine dust from the Xingjian's high-quality coal, and 0.1–2.2%$OP^{TOT}\cdot\mu g^{-1}$ for similar samples from underground coal mines (working lower coal quality in Southern and Southwestern China). Moreover, some OP analysis from PM_4 by Zazouli et al. (2021) in Alborz Coal Basin underground coal mines show also low levels of OP^{TOT} (0.4–1.0%$OP^{TOT}\cdot\mu g^{-1}$ of PM_4). In accordance with Zazouli et al. (2021), which also collect their samples in eight different locations of underground coal mines, OP^{TOT} average reached 0.7%$OP^{TOT}\cdot\mu g^{-1}$ of PM_4 in their OP analyses, a value close to the averages of this study, open-pit coal mine study (Trechera et al., 2021), and underground coal mines study (Trechera et al., 2020), reaching 1.2, 0.5 and 0.8%$OP^{TOT}\cdot\mu g^{-1}$, respectively. Thus, the results are quite similar, even when the OP from Zazouli et al. (2021) was measured on true respirable coal dust in suspension (PM_4), the ones from Trechera et al. (2020 and 2021) were obtained in respirable fractions extracted from deposited coal dust, and the ones from this study are CP_4 samples.

All the above values can be considered as relatively low when compared with those reported for other PM types. Thus, Moreno et al. (2017) reported 2.5%$OP^{TOT}\cdot\mu g^{-1}$ as average values from $PM_{2.5}$ samples collected in the Barcelona subway system. Calas et al. (2018) reported 1.5 and 4.0%$OP^{TOT}\cdot\mu g^{-1}$, respectively, for PM from the Chamonix Valley in summer and winter (the latter with high PM contributions from biomass burning). Godri et al. (2011) and Soltani et al. (2018) reported 1.1 and 3.6%$OP^{TOT}\cdot\mu g^{-1}$ at the Iranian Gol-E-Gohar mining and industrial facility and London Roadside PM control, respectively. It is also very relevant that ROS levels measured for coal mine dust by means of OP tests are somewhat reduced when compared with atmospheric PM from most anthropogenic sources (Trechera et al., 2020, 2021).

When evaluating correlations of the particle size, geochemical and mineralogical patterns of the 22 CP_4 samples with OP^{AA} (Fig. 3), a positively correlation (r = 0.69) with Fe, and with anatase, S, pyrite, U, Mo, V and Ti (r = 0.5–0.6) was found, as well as with Ni, Cu, Pb, ash yield, Al and Si (r = 0.4–0.5). On the other hand, OP^{GSH} was correlated with moisture (% ad, r = 0.67), and with H (%), volatile matter (% daf) and quartz (r = 0.4–0.5). Furthermore, OP^{DTT} was correlated with moisture, B, Ge, As and W (r = 0.5–0.6) and less correlated with particle size, volatile matter, and Ca (r = 0.4–0.5), Fig. 3.

Fig. 4 shows the cross-correlation analysis for CP_4 from bituminous coals (twelve out of the twenty-two samples analysed). OP^{AA} correlation increased slightly for Fe (r = 0.80), ash yield (r = 0.72) and pyrite (r = 0.70), as well as with sulphates, As, K, S, Si, Al, V, and Cr (r = 0.5–0.6) and Pb, Cu, Ti, U, and Ni (r = 0.4–0.5). For OP^{GSH} the correlation with moisture again markedly increased (r = 0.78), as did that with H, particle size, Sb, Bi, Tl, volatile matter, B, Ge and C (r = 0.3–0.5). For OP^{DTT}, correlations also increased for particle size, Ca, Sr, and B (r = 0.6–0.7), and for Mg, Mn, and quartz (r = 0.4–0.5). However, the correlation with Ge, W, As, Be, moisture content and volatile matter were decreased (the two latter being low in bituminous coal).

Accordingly, both OP^{GSH} and OP^{DTT} seem to correlate with the organic matter content (traced by moisture, H, volatile matter and by some typically organic associated trace elements, such as B, Mo, W and Ge (Swaine, 1990), and coarser particle size). In contrast, Figs. 3 and 4 clearly illustrate the mineral components (inorganic fraction) are linked to OP^{AA} (conversely to OP^{GSH} and OP^{DTT}), especially pyrite, Fe, S, sulphate minerals (arising from pyrite oxidation), anatase, and a number of trace metals (U, Mo, V). Most of these correlations increase when considering only bituminous coals, since the regression scatter caused by the possible impact of coal rank-dependent parameters is reduced. Attfield and Morring (1992), Castranova and Vallyathan (2000), Huang et al. (2005), Maclaren et al. (1989) and Huang et al. (1998) have showed that coal rank plays an important role in developing coal miners' diseases, with CWP risk increasing with rank.

Table 3
Contents of major and trace elements in the bulk coal channel profile samples (CP). wt, weight.

Sample	CP_01	CP_02	CP_03	CP_04	CP_05	CP_06	CP_07	CP_08	CP_09	CP_10	CP_11	CP_12	CP_13	CP_14	CP_15	CP_16	CP_17	CP_18	CP_19	CP_20	CP_21	CP_22
% wt																						
Al	1.16	1.19	2.78	0.32	0.57	2.96	2.91	3.37	3.82	2.60	2.02	2.99	4.33	1.85	0.87	1.98	4.55	0.06	0.18	0.09	2.85	1.50
Ca	1.31	0.91	0.97	0.63	0.57	0.16	0.53	2.91	0.07	0.16	0.09	0.53	0.75	0.03	1.87	0.05	0.78	6.40	0.38	1.35	0.42	0.39
Fe	0.52	0.11	0.99	1.41	0.94	1.69	0.27	4.59	8.04	6.10	0.99	1.43	0.54	2.27	3.60	1.01	0.89	1.48	0.09	0.13	2.05	0.59
K	0.09	0.04	0.24	0.02	0.05	0.03	0.14	0.17	0.40	0.12	0.11	0.07	0.14	0.37	0.18	0.10	0.87	<0.01	<0.01	<0.01	0.17	0.06
Mg	0.02	0.05	0.17	0.13	0.14	0.02	0.03	0.39	0.12	0.05	0.04	0.03	0.10	0.05	0.09	0.06	0.34	0.31	0.07	0.18	0.12	0.03
Na	0.01	0.02	0.10	0.03	0.03	0.02	0.02	0.02	0.02	0.01	0.03	0.04	0.01	0.14	0.02	0.14	0.01	0.01	0.17	0.06	0.01	0.01
P	<0.01	0.05	0.02	<0.01	<0.01	<0.01	0.02	0.02	0.01	0.02	0.02	0.40	0.01	<0.01	<0.01	0.01	0.01	<0.01	<0.01	<0.01	0.12	0.08
S	4.87	0.36	0.63	1.72	1.21	1.61	0.55	4.93	10.11	7.10	2.66	3.08	1.80	2.90	4.22	1.14	1.38	0.24	0.11	0.11	5.51	3.37
$mg \cdot kg^{-1}$																						
Li	68	33	16	2.9	4.2	25	35	70	52	46	44	36	70	31	9.0	162	31	0.97	<dl	<dl	12	3.4
Be	1.4	<dl	1.0	17	11	6.0	2.1	6.3	3.6	16	4.1	5.6	17	2.5	1.5	0.81	2.0	<dl	<dl	2.4	0.89	0.20
B	4.1	24	<dl	51	65	1.9	12	14	27	<dl	34	16	<dl	3.5	<dl	<dl	<dl	32	126	52	43	6.3
Sc	1.6	1.1	3.5	1.0	0.90	5.0	6.2	26	5.4	6.2	2.7	1.8	15	3.3	2.5	3.4	8.2	<dl	<dl	<dl	3.2	<dl
Ti	328	371	986	156	358	1045	1807	1709	2589	2027	786	483	2791	1835	558	661	1625	14	48	45	1111	718
V	7.5	6.6	18	4.5	7.1	15	35	53	268	65	15	21	94	199	65	20	93	<dl	0.94	<dl	116	51
Cr	4.4	4.1	11	2.9	4.6	5.4	9.9	51	79	25	9.9	14	41	46	7.9	8.8	61	<dl	0.96	0.52	30	12
Mn	19	23	148	49	48	97	29	82	154	13	10	27	8.6	8.4	235	4.1	11	721	12	18	36	6.1
Co	1.6	2.5	4.4	0.92	1.0	8.3	2.8	9.0	10	12	3.3	14	6.6	7.1	6.4	5.4	6.6	<dl	1.5	8.7	2.7	<dl
Ni	2.2	7.4	11	2.5	2.2	13	4.3	69	33	16	8.2	16	36	22	12	11	32	0.56	4.3	5.1	22	20
Cu	4.5	6.8	16	3.0	4.5	16	17	55	22	39	13	24	52	54	30	21	43	<dl	0.64	1.2	20	19
Zn	8.9	22	21	6.9	13	24	26	2446	24	14	57	28	14	17	2.5	9.6	19	<dl	<dl	<dl	48	35
Ga	5.0	3.9	9.2	1.7	1.8	10	16	51	14	36	10	13	52	8.8	3.8	7.6	12	<dl	<dl	2.2	7.9	5.1
Ge	3.2	1.1	2.1	577	436	3.2	2.0	11	3.9	15	5.8	18	17	1.6	0.79	1.0	2.6	<dl	<dl	3.7	22	4.4
As	1.6	1.1	3.1	484	436	9.8	2.9	36	29	36	4.0	6.6	8.5	3.0	5.7	1.6	8.4	<dl	<dl	1.3	225	65
Se	0.64	1.2	1.8	<dl	<dl	2.2	2.5	21	6.0	17	2.8	8.5	16	2.2	1.9	1.8	2.5	<dl	<dl	<dl	5.4	5.0
Rb	3.9	0.89	16	1.4	3.6	0.92	5.5	4.6	10	3.4	2.7	2.5	3.8	15	3.9	3.2	89	<dl	<dl	<dl	38	10
Sr	63	239	432	51	47	33	185	149	138	81	358	3770	118	54	1014	90	25	792	95	532	98	23
Y	4.8	8.6	15	1.5	2.0	17	17	200	21	80	16	33	110	14	9.6	16	16	<dl	<dl	7.1	12	5.7
Zr	18	9.8	40	3.9	6.4	50	132	1888	122	296	69	91	735	100	14	22	38	<dl	1.3	1.1	24	19
Nb	1.8	1.8	6.4	0.75	1.2	5.3	7.7	144	24	54	18	25	90	23	2.2	3.1	5.9	<dl	<dl	<dl	3.5	5.0
Mo	1.8	<dl	<dl	<dl	<dl	<dl	2.2	8.2	160	16	2.7	3.3	2.7	122	7.2	<dl	<dl	<dl	<dl	<dl	138	402
Sn	0.48	<dl	1.3	<dl	<dl	1.4	1.4	5.8	3.2	3.6	1.2	1.3	11	1.4	0.39	0.80	1.8	<dl	<dl	<dl	<dl	<dl
Sb	<dl	<dl	1.1	27	20	<dl	<dl	8.8	1.9	0.65	<dl	<dl	0.95	<dl	<dl	<dl	14	<dl	<dl	4.4	29	7.6
Cs	<dl	<dl	2.2	4.6	5.2	<dl	<dl	0.81	0.84	<dl	<dl	<dl	<dl	<dl	<dl	<dl	13	<dl	<dl	<dl	49	23
Ba	1.7	37	151	26	21	21	39	8.0	25	6.0	18	34	8.8	90	33	31	146	5.4	23	6.4	170	37
Hf	0.94	<dl	2.1	<dl	<dl	2.6	5.9	47	5.2	12	2.9	4.0	25	4.0	<dl	1.2	2.0	<dl	<dl	<dl	<dl	<dl
W	1.2	<dl	0.58	461	447	5.1	1.7	0.79	1.1	0.94	<dl	1.1	0.66	0.99	<dl	<dl	0.72	<dl	<dl	<dl	9.6	1.5
Pb	3.1	8.6	16	0.43	0.67	112	22	95	25	155	3.4	3.9	17	8.4	1.9	4.8	15	<dl	<dl	<dl	15	13
Th	1.9	1.1	11	<dl	0.82	7.2	10	8.6	5.5	9.1	3.6	2.7	12	3.9	1.3	2.8	8.3	<dl	<dl	<dl	4.7	2.9
U	0.81	<dl	4.4	<dl	<dl	2.3	2.8	7.4	45	4.7	2.1	3.6	11	51	1.5	1.0	11	<dl	<dl	<dl	81	73
REE	28	88	104	8.0	10	91	116	991	189	760	203	311	629	85	51	88	73	1.2	1.0	17	54	33

Table 4
Mineral contents (%wt) in the fraction <4 μm of the powdered samples from the channel profiles (CP_4). Qtz, Quartz; Ant, Anatase; Cb, Carbonates; Py, Pyrite; Sul, Sulphates; Ill-Ms, Illite-Muscovite; Mm, Montmorillonite; Kln-Clc, Kaolinite-Clinochlore; Tob, Tobelite; Ank, Ankerite; Cal, Calcite; Dol, Dolomite; Sid, Siderite; Gy, Gypsum; Jar, Jarosite; Szo, Szomolnokite; Roz, Rozenite; Mel, Melanterite.

Sample	CP_4_01	CP_4_02	CP_4_03	CP_4_04	CP_4_05	CP_4_06	CP_4_07	CP_4_08	CP_4_09	CP_4_10	CP_4_11	CP_4_12	CP_4_13	CP_4_14	CP_4_15	CP_4_16	CP_4_17	CP_4_18	CP_4_19	CP_4_20	CP_4_21	CP_4_22
Clays	5.4	3.2	11.7	<dl	4.3	12.9	4.6	5.8	8.9	4.3	7.8	9.7	14.9	9.0	<dl	15.0	18.9	0.1	1.4	<dl	16.4	13.9
Qtz	<dl	<dl	7.2	4.0	3.2	<dl	1.3	0.6	1.7	0.1	<dl	<dl	<dl	2.4	2.2	<dl	29.6	<dl	0.5	11.9	8.3	7.7
Ant	<dl	<dl	<dl	<dl	<dl	<dl	<dl	<dl	<dl	<dl	<dl	<dl	<dl	0.9	0.5	0.9	<dl	<dl	<dl	<dl	1.1	0.8
Cb	1.3	2.1	5.2	<dl	<dl	1.1	2.1	9.2	<dl	<dl	<dl	0.2	1.7	<dl	3.2	<dl	<dl	14.4	2.0	<dl	<dl	<dl
Py	0.3	0.1	0.5	2.4	0.6	0.7	<dl	3.4	9.5	8.1	0.7	2.7	0.2	7.5	2.3	0.5	2.5	0.1	<dl	<dl	2.5	1.2
Sul	0.1	<dl	<dl	1.5	1.3	0.1	<dl	0.3	3.7	2.2	<dl	0.3	<dl	1.1	1.5	<dl	<dl	<dl	<dl	<dl	<dl	<dl
Ill-Ms	<dl	<dl	<dl	<dl	<dl	<dl	<dl	<dl	<dl	<dl	<dl	<dl	<dl	<dl	<dl	0.9	4.6	<dl	<dl	<dl	<dl	<dl
Mm	<dl	<dl	<dl	<dl	<dl	<dl	<dl	<dl	<dl	<dl	<dl	<dl	<dl	5.3	<dl	<dl	<dl	<dl	<dl	<dl	<dl	<dl
Kln-Clc	2.1	1.9	11.7	<dl	4.3	12.9	4.6	5.8	8.9	4.3	1.9	1.5	14.9	<dl	<dl	14.1	14.4	0.1	1.4	<dl	<dl	<dl
Tob	3.3	1.4	<dl	<dl	<dl	<dl	<dl	<dl	<dl	<dl	5.9	8.1	<dl	3.7	<dl	<dl	<dl	<dl	<dl	<dl	16.4	13.9
Ank	<dl	0.1	0.3	<dl	<dl	<dl	<dl	1.2	<dl	<dl	<dl	<dl	<dl	<dl	<dl	<dl	<dl	0.8	<dl	<dl	<dl	<dl
Cal	1.3	1.9	4.6	<dl	<dl	<dl	2.1	7.5	<dl	<dl	<dl	<dl	1.6	<dl	3.2	<dl	<dl	13.1	2.0	<dl	<dl	<dl
Dol	<dl	<dl	<dl	<dl	<dl	<dl	<dl	<dl	<dl	<dl	<dl	<dl	0.1	<dl	<dl	<dl	<dl	<dl	<dl	<dl	<dl	<dl
Sid	<dl	<dl	0.3	<dl	<dl	1.1	<dl	0.5	<dl	<dl	<dl	0.2	<dl	<dl	<dl	<dl	<dl	0.5	<dl	<dl	<dl	<dl
Gy	0.1	<dl	<dl	1.5	1.3	<dl	<dl	0.1	<dl	0.2	<dl	<dl	<dl	<dl	<dl	<dl	<dl	<dl	<dl	<dl	<dl	<dl
Jar	<dl	<dl	<dl	<dl	<dl	<dl	<dl	<dl	<dl	<dl	<dl	0.3	<dl	<dl	<dl	<dl	<dl	<dl	<dl	<dl	<dl	<dl
Szo	<dl	<dl	<dl	<dl	<dl	<dl	<dl	<dl	2.2	1.5	<dl	<dl	<dl	<dl	1.5	<dl	<dl	<dl	<dl	<dl	<dl	<dl
Roz	<dl	<dl	<dl	<dl	<dl	<dl	<dl	<dl	1.6	0.3	<dl	<dl	<dl	1.1	<dl	<dl	<dl	<dl	<dl	<dl	<dl	<dl
Mel	<dl	<dl	<dl	<dl	<dl	0.1	<dl	0.1	<dl	0.1	<dl	<dl	<dl	<dl	<dl	<dl	<dl	<dl	<dl	<dl	<dl	<dl

3.2.2. Correlation analysis of OP and geochemical patterns including CP_4 actual respirable coal mine dust samples

Figs. 5 and 6 show the results of the cross-correlation analysis of OP with geochemical, mineralogical and particle size of CP_4 samples but, in this case, adding recently respirable coal mine dust (RD) from Chinese mines, sampled and characterised using the same methodology by Trechera et al. (2020, 2021). The information on the origin and features of the RD samples included is supplied in Table S4. This re-analysis is done with the aim to validate the procedure to study the possible OP from mining dust of a given coal by sampling the coal seam, powdering the coal and extracting the CP_4. Thus, the main results obtained for CP_4, which remain valid in the re-analysis by including RD, will support the validation of the protocol used in this study.

There, again correlation was found for S, U, Mo and pyrite (r = 0.6–0.5) with OP^{AA} (Fig. 5). However, in spite of the correlation of OP^{AA} with pyrite, the OP^{AA}-Fe correlation markedly decreased (r = 0.39) when all samples were combined (CP_4 and RD). On the other hand, moisture (r = 0.52) and some elements and minerals, such as Ca, Na, carbonates (r = 0.3–0.4) and B (r = 0.20) correlated with OP^{GSH}. By including actual coal mine dust samples in the correlation analysis, some high calcite, Na and As dust from galleries with limegunited walls that interacted with acid drainage waters (Trechera et al., 2020) seem to increase correlation with OP^{GSH}; and Na and Mg (r = 0.6–0.5) and moisture (r = 0.40) with OP^{DTT} (Fig. 5). Furthermore, by including RD samples elements such as K, Si, Rb, Sb, Ge, W, As, and Ba markedly decreased their correlation with OP^{DTT}.

Again, OP correlations increased when the analysis focused only on bituminous coal and coal dust samples (Fig. 6). There, an increase was found for correlation of ash yield, sulphates, anatase, Ti, Ni, Co, V, Pb and REEs with OP^{AA}, but the most noticeable increase was found for Fe (r = 0.83) and pyrite (r = 0.66). Thus, Fe-OP^{AA} correlation is very high when CP_4 and RD are analysed together for bituminous coals. For OP^{GSH} and OP^{DTT}, elements such as Ca, Na, Mg, B, Bi, Tl, and Sr, PSD, moisture content and quartz mineral also increase correlations. Moisture-OP^{GSH} (r = 0.73) and Mg-OP^{DTT} (r = 0.70) markedly increased in this combined analysis. Conversely, U and Mo correlation with OP^{AA} decreased when only bituminous coal was considered.

According to this re-analysis, OP correlations remain or even increase when RD samples for Fe, pyrite, S, sulphates, moisture content or B are included, and also, to a lesser extent, with elements such as U, Mo, V, Ti, Ni, K, Si, Pb, Co, Sb, Bi, As, W, Ge, Ca, Na, Mg and Mn; and minerals such as anatase, quartz or carbonates, ash yield, and particle size.

The results obtained between the OP and respirable fractions from CP_4 analysis samples of given coal might yield information on the expected OP of the RD of the coal when some working operations are carried out in the coal mines. In conclusion, the evaluation of OP coal worked in coal mines could offer insight into which elements could be more problematic in coal mines or which parameters are more potentially hazardous in coal mines.

3.2.3. Multilinear regression analysis

Figs. S3 and S4 and Eqs. (1) to (22) summarise the results of the multilinear regression analysis performed for the OP^{AA}, OP^{GSH}, and OP^{DTT} with geochemical parameters for the combined CP_4 and RD dataset. It has to be pointed out that a number of components are included in the equations for OP^{AA}, OP^{GSH}, and OP^{DTT} although they have opposite effects.

All coal and dust samples (n = 43), Fig. S3

$$OP^{AA}\ (\%\cdot\mu g^{-1}) = 0.11 * \text{pyrite}\ (\%wt) + 0.09 * \text{sulphates}\ (\%wt) - 0.07 * \text{moisture content}\ (\%ad) + 0.74\ (r = 0.70; \rho < 0.0001) \quad (1)$$

Table 5
Contents of major and trace elements in the fraction <4 μm of the powdered samples of the coal channel profiles (CP_4). wt, weight.

Sample	CP_4_01	CP_4_02	CP_4_03	CP_4_04	CP_4_05	CP_4_06	CP_4_07	CP_4_08	CP_4_09	CP_4_10	CP_4_11	CP_4_12	CP_4_13	CP_4_14	CP_4_15	CP_4_16	CP_4_17	CP_4_18	CP_4_19	CP_4_20	CP_4_21	CP_4_22
% wt																						
Al	1.22	0.83	3.59	0.44	0.83	2.80	1.22	3.20	3.57	2.21	1.66	2.46	3.39	3.06	0.84	3.26	6.04	0.12	0.42	0.11	3.95	3.67
Si	1.18	0.82	5.60	0.86	1.90	2.90	1.33	3.73	4.51	2.47	1.85	2.46	3.84	4.02	1.62	3.38	9.44	0.10	0.43	0.14	7.07	5.35
Ca	0.47	0.57	0.72	0.71	0.76	0.13	0.43	1.06	0.14	0.24	0.07	0.38	0.24	0.21	0.95	0.08	0.83	6.76	0.41	1.43	0.52	0.36
Fe	0.27	0.04	1.10	0.76	0.88	1.08	0.18	1.05	4.08	2.55	0.18	0.32	0.19	3.30	1.61	0.75	0.94	1.25	0.11	0.13	2.36	0.58
K	0.09	0.04	0.37	0.02	0.06	<0.01	0.06	0.16	0.34	0.09	0.07	0.05	0.11	0.63	0.16	0.14	1.14	0.01	<0.01	<0.01	0.27	0.13
Mg	0.02	0.03	0.20	0.15	0.17	0.02	0.04	0.18	0.12	0.05	0.04	0.03	0.08	0.09	0.06	0.09	0.44	0.20	0.08	0.20	0.16	0.03
Na	0.03	0.02	0.13	0.05	0.04	0.02	0.02	0.02	0.03	0.02	0.03	0.04	0.02	0.22	0.03	0.21	0.03	0.02	0.15	0.06	0.03	0.01
P	<0.01	0.05	0.02	<0.01	<0.01	<0.01	0.01	0.02	0.02	0.01	0.02	0.31	0.01	0.01	<0.01	0.01	0.01	<0.01	<0.01	<0.01	0.13	0.09
S	5.30	0.35	0.70	1.00	1.07	1.05	2.55	1.46	6.22	4.78	1.62	2.02	1.50	3.68	2.71	0.74	1.25	0.25	0.10	0.12	5.45	1.34
$mg \cdot kg^{-1}$																						
Li	69	21	18	4.3	5.0	18	9.9	56	30	28	27	25	47	41	5.6	193	36	<dl	1.0	<dl	7.8	30
Be	1.0	<dl	<dl	16	17	5.7	2.3	5.8	4.3	5.2	1.6	3.6	12	2.5	<dl	0.89	2.6	<dl	<dl	2.2	2.0	0.89
B	24	27	3.3	47	36	19	12	18	64	7.8	8.1	18	<dl	<dl	7.3	<dl	<dl	32	73	45	23	11
Sc	1.6	1.2	4.2	0.91	1.0	6.1	5.6	27	6.2	6.0	2.5	1.6	14	4.2	2.5	3.7	9.3	<dl	<dl	<dl	5.0	3.8
Ti	287	398	992	163	337	854	1016	1702	2390	1687	608	425	2418	1603	518	645	1663	12	34	18	1289	1450
V	7.8	7.2	26	3.9	6.5	16	38	59	269	65	13	21	94	246	66	24	84	0.75	0.76	<dl	95	42
Cr	4.8	4.6	16	2.8	4.5	6.3	15	34	76	24	9.5	14	40	53	8.9	8.9	64	<dl	0.45	<dl	35	9.3
Mn	6.8	11	78	47	46	86	23	26	74	7.3	4.9	11	3.3	23	102	5.1	12	640	14	16	32	7.0
Co	1.5	2.4	5.1	0.88	0.94	7.1	2.6	7.0	9.7	6.4	2.0	11	5.5	10	5.3	5.1	5.1	<dl	1.7	9.6	4.1	3.4
Ni	1.2	7.2	14	1.2	1.4	11	4.8	55	34	8.5	4.2	13	33	38	6.5	5.7	30	<dl	2.5	3.5	21	22
Cu	4.1	4.1	20	3.2	5.8	12	12	34	15	18	6.1	11	31	63	24	20	41	3.1	2.5	2.6	21	20
Zn	19	38	48	14	17	18	26	526	40	27	28	27	29	33	23	15	24	10	16	12	45	37
Ga	5.4	3.3	9.8	1.3	1.6	8.7	13	43	9.6	24	7.4	9.2	41	14	3.5	10	14	<dl	<dl	1.5	9.3	7.0
Ge	2.7	0.85	1.9	315	211	2.2	19	11	3.2	6.4	3.8	14	12	2.0	<dl	1.2	1.8	<dl	<dl	1.4	20	1.8
As	1.8	3.5	3.5	389	495	12	14	18	18	24	3.1	22	5.8	5.7	7.5	1.8	7.7	0.53	0.47	1.3	249	58
Se	0.72	<dl	2.2	<dl	<dl	1.5	2.3	19	3.7	12	2.7	6.2	11	3.3	1.2	2.2	2.2	<dl	<dl	<dl	2.4	1.2
Rb	4.8	<dl	25	2.1	5.0	<dl	4.3	4.3	7.5	2.6	2.0	1.9	3.2	25	3.5	4.5	110	<dl	<dl	<dl	46	10
Sr	54	226	319	52	55	31	140	110	125	77	278	3308	104	127	499	163	30	767	92	500	124	156
Y	4.0	6.7	13	1.4	1.9	16	10	181	22	65	12	25	93	14	7.6	15	13	<dl	<dl	5.8	15	14
Zr	27	17	57	4.9	9.3	66	107	3335	184	512	97	132	1174	141	25	31	53	<dl	1.3	<dl	29	104
Nb	1.5	2.0	5.9	<dl	0.86	3.9	5.1	140	21	48	14	22	81	18	2.0	3.0	5.9	<dl	<dl	<dl	4.0	6.3
Mo	3.8	0.86	2.2	<dl	<dl	0.97	21	3.2	79	5.8	2.2	2.8	2.6	98	2.8	<dl	<dl	<dl	<dl	<dl	41	115
Sn	0.38	0.77	1.7	<dl	0.70	1.6	1.2	6.2	2.5	4.0	1.5	4.5	10	1.5	<dl	0.88	2.0	<dl	<dl	<dl	1.8	1.7
Sb	<dl	3.3	1.3	20	16	<dl	7.4	5.8	<dl	<dl	<dl	23	0.79	0.84	0.84	<dl	11	<dl	<dl	2.8	31	0.79
Cs	<dl	<dl	3.9	6.8	9.3	<dl	4.1	<dl	<dl	<dl	<dl	<dl	<dl	1.1	<dl	<dl	17	<dl	<dl	<dl	56	15
Ba	1.7	35	187	34	37	20	38	11	21	7.3	11	30	9.7	157	35	59	211	6.0	27	6.6	270	41
Hf	0.74	<dl	1.5	<dl	<dl	1.9	2.5	39	4.5	9.1	2.1	3.2	19	3.2	<dl	0.90	1	<dl	<dl	<dl	0.80	2.6
W	1.7	<dl	1.3	406	360	3.4	2.8	1.6	<dl	1.3	0.87	1.6	1.1	1.8	<dl	<dl	1.4	<dl	<dl	<dl	8.1	0.76
Pb	2.5	8.3	17	<dl	0.88	122	20	38	7.8	117	1.1	1.9	14	5.1	1.8	4.7	16	0.86	0.97	0.58	11	6.6
Th	2.1	1.3	13	<dl	0.99	8.1	9.4	7.2	5.2	7.0	3.7	2.6	9.7	5.0	1.5	3.8	11	<dl	<dl	<dl	5.0	6.2
U	0.91	<dl	5.4	<dl	<dl	2.4	5.8	8.6	48	5.1	2.0	4.2	12	99	2.0	1.3	10	<dl	<dl	<dl	79	59
REE	27	89	114	9.5	13	78	91	1026	158	552	171	275	530	153	44	111	82	2.0	1.0	17	75	74

Table 6
Most geochemical interesting and enrichments elements and high concentrations of bulk channel profile (CP) coals in comparison with Chinese geochemical averaged concentrations (Dai et al., 2007, 2008). LV, Low-Volatile; HV, High-Volatile; MV, Medium-Volatile.

Sample	Ash yield	Rank	Interesting elements	Trace elements ($mg \cdot kg^{-1}$)
CP_01	Medium	LV bituminous	High organic S, low Fe and pyrite	Low levels
CP_02	Medium	Semi-anthracite	Low S	Low levels
CP_03	High	HV bituminous		Sr (432), Th (11)
CP_04	Medium	Sub-bituminous		Ge (577), As (484), W (461), Sb (27), Be (17), Cs (5.2)
CP_05	Medium	Sub-bituminous		Ge (436), As (436), W (447), Sb (20), Be (11), Cs (5.2)
CP_06	High	HV bituminous		Pb (112), Be (6.0), As (9.8), W (5.1)
CP_07	High	HV bituminous	Anatase mineral detected by XRD (High Ti)	Th (10)
CP_08	High	MV bituminous	High pyrite	Zn (2446), Zr (1888), Cd, Pb, Cr, Ni, Cu, Ga (51–95), As (36) Se (21), Y (200), Nb (144), REE's (991)
CP_09	High	MV bituminous	High S, Fe and pyrite	V (268), Mo (160), Cr (79), U (45), As (29)
CP_10	High	LV bituminous	High S, Fe and pyrite; Anatase mineral detected by XRD (High Ti)	Pb (155), As (36), Se (17), Y (80), Nb (54), REE's (760)
CP_11	Medium	Semi-anthracite		Sr (358)
CP_12	High	Semi-anthracite	High P	Sr (3770)
CP_13	High	LV bituminous	Anatase mineral detected by XRD (High Ti)	Ti (2791), Y (110), Zr (735), REE (629), Th (12)
CP_14	Medium	Anthracite	Anatase mineral detected by XRD (High Ti)	Mo (122), V (199), U (51)
CP_15	High	LV bituminous		Sr (1014), Mn (235)
CP_16	Medium	Anthracite		Li (162)
CP_17	High	Lignite	High quartz, kaolinite-chlorite and illite minerals; Anatase mineral detected by XRD (High Ti)	Cr, Rb, Cu, Ni (32–89)
CP_18	Medium	HV bituminous	High Ca and carbonates minerals	Mn (721), Sr (792)
CP_19	Low	HV bituminous		B (126)
CP_20	Low	HV bituminous		Sr (532)
CP_21	High	Semi-anthracite	High organic S	As (225), Mo (138), Sb (29), U (81)
CP_22	Medium	Semi-anthracite	High organic S	As (65), Mo (402), Sb (7.6), U (73), Tl (25)

$$OP^{AA}\ (\%\cdot\mu g^{-1}) = 0.13 * S\ (\%wt) + 0.01 * Mo\left(mg\cdot kg^{-1}\right) - 0.05 * \text{moisture content}\ (\%ad) + 0.65\ (r = 0.69; \rho < 0.0001) \quad (2)$$

$$OP^{AA}\ (\%\cdot\mu g^{-1}) = 0.19 * Fe\ (\%wt) + 0.01 * U\left(mg\cdot kg^{-1}\right) - 1.22 * Na\ (\%wt) + 0.64\ (r = 0.70; \rho<0.001) \quad (3)$$

$$OP^{AA}\ (\%\cdot\mu g^{-1}) = 0.12 * \text{pyrite}\ (\%wt) + 0.42 * \text{anatase}\ (\%wt) - 1.81 * Mg\ (\%wt) + 0.80\ (r = 0.73; \rho<0.0001) \quad (4)$$

$$OP^{GSH}\ (\%\cdot\mu g^{-1}) = 0.02 * \text{moisture content}\ (\%ad) + 0.02 * Ca\ (\%wt) - 0.03 * D_{25}(\mu m) + 0.15\ (r = 0.71; \rho<0.0001) \quad (5)$$

$$OP^{GSH}\ (\%\cdot\mu g^{-1}) = 0.02 * \text{moisture content}\ (\%ad) + 0.004 * \text{carbonates}\ (\%wt) + 0.09\ (r = 0.65; \rho<0.0001) \quad (6)$$

$$OP^{DTT}\ (\%\cdot\mu g^{-1}) = 1.45 * Mg\ (\%wt) + 0.98 * Na\ (\%wt) + 0.002 * Ge\left(mg\cdot kg^{-1}\right) + 0.52\ (r = 0.71; \rho<0.0001) \quad (7)$$

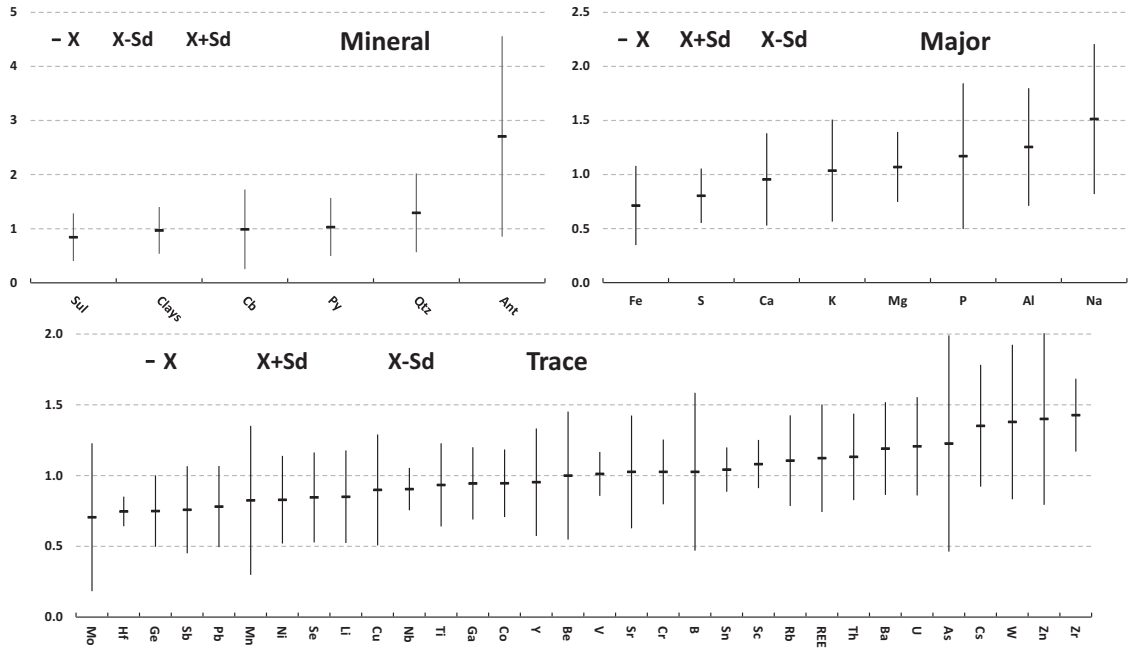

Fig. 2. Average ratio of mineral and major and trace element contents in the channel profile ¨4 μm (CP_4) and bulk channel profile (CP) samples. Ratio average (X) = CP_4/CP; Sd, Standard Deviation; Sul, Sulphates; Cb, Carbonates; Py, Pyrite; Qtz, Quartz; Ant, Anatase.

Table 7
Oxidative potential (OP) of the fraction <4 μm of the powdered channel profile samples (CP_4). AA, Ascorbic Acid; Sd, Standard deviation; GSH, Glutathione; TOT = AA+GSH; DTT, Dithiothreitol; **, insufficient sample for OP analysis.

Sample	$\%OP^{AA}$ μg^{-1}	Sd^{AA}	$\%OP^{GSH}$ μg^{-1}	Sd^{GSH}	$\%OP^{TOT}$ μg^{-1}	$\%OP^{DTT}$ μg^{-1}	Sd^{DTT}
CP_4_01	0.99	0.04	0.10	0.08	1.09	0.71	0.00
CP_4_02	0.42	0.01	0.25	0.06	0.68	0.88	0.00
CP_4_03	1.27	0.02	0.03	0.04	1.30	0.22	0.00
CP_4_04	0.24	0.03	0.19	0.08	0.42	1.88	0.00
CP_4_05	0.31	0.01	0.24	0.02	0.55	0.90	0.00
CP_4_06	1.50	0.07	0.18	0.03	1.68	0.50	0.00
CP_4_07	0.34	0.01	0.26	0.01	0.60	0.22	0.00
CP_4_08	1.49	0.02	0.16	0.01	1.65	0.44	0.00
CP_4_09	1.86	0.00	0.03	0.02	1.89	**	**
CP_4_10	1.80	0.00	0.09	0.03	1.89	0.22	0.00
CP_4_11	0.79	0.01	0.12	0.04	0.91	0.76	0.00
CP_4_12	0.65	0.04	0.01	0.05	0.66	0.38	0.00
CP_4_13	0.62	0.01	0.15	0.06	0.77	0.50	0.00
CP_4_14	1.60	0.02	0.09	0.03	1.69	0.68	0.00
CP_4_15	1.75	0.03	0.06	0.02	1.81	0.54	0.00
CP_4_16	1.47	0.04	0.11	0.06	1.58	0.62	0.00
CP_4_17	0.19	0.01	0.28	0.08	0.47	0.77	0.00
CP_4_18	1.04	0.02	0.12	0.08	1.16	1.22	0.00
CP_4_19	0.16	0.09	0.27	0.15	0.43	0.85	0.00
CP_4_20	0.12	0.00	0.28	0.08	0.40	1.41	0.00
CP_4_21	1.90	0.02	0.11	0.04	2.00	0.82	0.00
CP_4_22	1.78	0.00	0.16	0.06	1.94	0.56	0.00

$$OP^{DTT}\ (\%\cdot\mu g^{-1}) = 1.43 * Mg\ (\%wt) + 0.96 * Na\ (\%wt) + 0.002 * W\left(mg\cdot kg^{-1}\right) + 0.54\ (r = 0.70; \rho<0.0001) \quad (8)$$

$$OP^{DTT}\ (\%\cdot\mu g^{-1}) = 0.002 * Ba\left(mg\cdot kg^{-1}\right) + 0.04 * \text{moisture content}\ (\%, ad) - 0.05 * Th\left(mg\cdot kg^{-1}\right) + 0.86\ (r = 0.68; \rho = 0.0001)$$

Bituminous coals and Bituminous coal dust (n = 23), Fig. S4

$$OP^{AA}\ (\%\cdot\mu g^{-1}) = 0.36 * \text{anatase}\ (\%wt) + 0.15 * \text{pyrite}\ (\%wt) - 0.05 * \text{moisture content}\ (\%ad) + 0.71\ (r = 0.83; \rho = 0.0001) \quad (10)$$

$$OP^{AA}\ (\%\cdot\mu g^{-1}) = 0.44 * Fe\ (\%wt) + 0.04 * \text{carbonates}\ (\%wt) - 1.81 * Mg\ (\%wt) + 0.55\ (r = 0.90; \rho<0.0001) \quad (11)$$

$$OP^{AA}\ (\%\cdot\mu g^{-1}) = 0.64 * Fe\ (\%wt) + 0.01 * Li\left(mg\cdot kg^{-1}\right) - 0.01 * V\left(mg\cdot kg^{-1}\right) + 0.28\ (r = 0.91; \rho<0.0001) \quad (12)$$

$$OP^{AA}\ (\%\cdot\mu g^{-1}) = 0.48 * Al\ (\%wt) + 0.0003 * Ti\left(mg\cdot kg^{-1}\right) - 0.11 * \text{clays}\ (\%wt) + 0.50\ (r = 0.80; \rho<0.0001) \quad (13)$$

$$OP^{AA}\ (\%\cdot\mu g^{-1}) = 0.15 * \text{pyrite}\ (\%wt) + 0.08 * \text{sulphate}\ (\%wt) - 0.01 * B\left(mg\cdot kg^{-1}\right) + 0.87\ (r = 0.83; \rho = 0.0001) \quad (14)$$

$$OP^{AA}\ (\%\cdot\mu g^{-1}) = 0.04 * \text{ash yield}\ (\%db) + 0.01 * Pb\left(mg\cdot kg^{-1}\right) - 0.07 * \text{clays}\ (\%wt) + 0.36\ (r = 0.81; \rho = 0.0001) \quad (15)$$

$$OP^{GSH}\ (\%\cdot\mu g^{-1}) = 0.027 * \text{moisture content}\ (\%ad)\ (r = 0.85; \rho<0.0001) \quad (16)$$

$$OP^{GSH}\ (\%\cdot\mu g^{-1}) = 0.003 * B\left(mg\cdot kg^{-1}\right) + 0.0001 * Ti\left(mg\cdot kg^{-1}\right) - 0.002 * V\left(mg\cdot kg^{-1}\right) + 0.092\ (r = 0.76; \rho = 0.001) \quad (17)$$

$$OP^{GSH}\ (\%\cdot\mu g^{-1}) = 0.020 * Bi\left(mg\cdot kg^{-1}\right) + 0.003 * B\left(mg\cdot kg^{-1}\right) - 0.003 * Mo\left(mg\cdot kg^{-1}\right) + 0.071\ (r = 0.76; \rho = 0.001) \quad (18)$$

$$OP^{DTT}\ (\%\cdot\mu g^{-1}) = 3.29 * Mg\ (\%wt) - 0.06 * Th\left(mg\cdot kg^{-1}\right) + 0.71\ (r = 0.85; \rho<0.0001) \quad (19)$$

$$OP^{DTT}\ (\%\cdot\mu g^{-1}) = 1.28 * Na\ (\%wt) + 0.06 * \text{quartz}\ (\%wt) + 0.001 * Mn\left(mg\cdot kg^{-1}\right) + 0.42\ (r = 0.85; \rho = 0.001) \quad (20)$$

$$OP^{DTT}\ (\%\cdot\mu g^{-1}) = 0.04 * \text{moisture content}\ (\%ad) + 0.09 * \text{quartz}\ (\%wt) - 0.13 * Cs\left(mg\cdot kg^{-1}\right) + 0.60\ (r = 0.75; \rho = 0.002) \quad (21)$$

$$OP^{DTT}\ (\%\cdot\mu g^{-1}) = 0.01 * B\left(mg\cdot kg^{-1}\right) + 0.07 * \text{quartz}\ (\%wt) - 0.03 * Mo\left(mg\cdot kg^{-1}\right) + 0.56\ (r = 0.76; \rho = 0.002) \quad (22)$$

Thus, as shown by these equations, Fig. S3 and Fig. S4, Fe, pyrite and sulphate minerals (indicating acidic species from pyrite oxidation), followed by anatase and, in a much lower proportion, U, Mo, V and Pb, clearly govern the OP^{AA}; while moisture content, Ca, carbonate minerals, coarse particle size and B control OP^{GSH}; whereas Mg, Na, quartz, B, moisture content and Ba regulate OP^{DTT}.

3.2.4. Interpretation of links between geochemical patterns of samples and oxidative potential

3.2.4.1. Ascorbic acid oxidative potential (OP^{AA}). As stated above, Fe and pyrite are most strongly linked to OP^{AA} in the CP_4 and RD samples studied, and this relationship increases when only bituminous coals rank species are evaluated. Cohn et al. (2006b), Liu and Liu (2020), and R. Zhang et al. (2021) found that ROS generation is strongly linked with Fe and pyrite contents in coal. Harrington et al. (2012) reported that pyrite particles may remain in the lungs for a year or more, generating ROS in cells and potentially contributing to the pathogenesis of CWP. Thus, the results indicate that special controls should be implemented for working and handling high pyrite coals to reduce the occupational health impacts.

Huang et al. (1998) defined bioavailable Fe (BAI) as free-Fe in a 10 mM phosphate solution, pH 4.5 - which is the pH of the phagolysosomes of lung macrophages. They proposed this BAI as a marker of the potential of the dust to induce CWP. Coal workers' exposure to coal dust that contains acid-soluble Fe with low buffering capacity coal (low carbonate minerals in coal) would be more likely to induce oxidative stress, leading to lung injury and CWP development. This is in contrast to high buffering capacity coal exposure, which renders the coal less hazardous. Huang et al. (2005) reported a strong correlation for BAI values and CWP cases for bituminous coal mining areas of the United States, as well as was the correlation with the content of sulphate and pyrite sulphur. Furthermore, Harrington et al. (2012) documented the role of inhaled pyrite particles in promoting CWP pathogenesis. Regular exposure to coal dust containing pyrite mineral is predicted to lead to a build-up of pyrite in the lung that will slowly disappear over a time

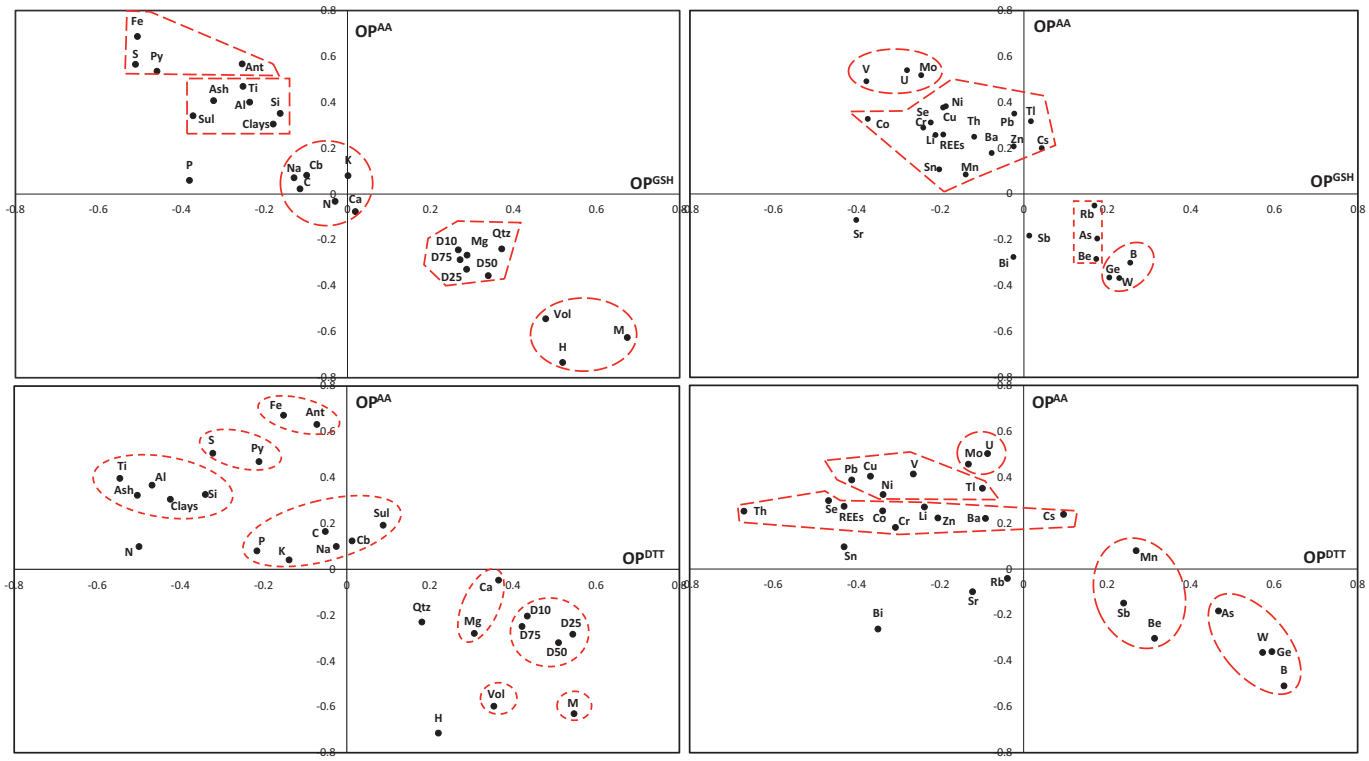

Fig. 3. Cross-correlation plots between the Pearson's correlation coefficients of geochemical parameters of all (22) channel profile samples <4 μm (CP_4) (mineralogy, chemistry, size, and proximate analysis) with their respective OP^{AA} vs OP^{GSH}, and OP^{AA} vs OP^{DTT}. Py, Pyrite; Ant, Anatase; Sul, Sulphates; Cb, Carbonates; Qtz, Quartz; D_{10}, D_{25}, D_{50}, D_{75}, percentiles 10, 25, 50 and 75 of the particle size in μm, respectively; Vol, Volatile Matter; M, Moisture.

scale of years. Moreover, frequent exposure to respirable pyrite particles in coal dust over years promotes a chronic level of inflammation, developing hydrogen peroxide and ferrous-Fe, which produce highly reactive hydroxyl radicals, potentially contributing to the pathogenesis of CWP (Cohn et al., 2006b; Harrington et al., 2012). In addition, other minerals in coal dust, such as quartz, have been shown to promote CWP pathogenesis, but none of these minerals could generate hydroxyl radicals at the same level as pyrite (Cohn et al., 2006a; Harrington et al., 2012). Moreover, Yu et al. (2020) state that several metals, including Fe, are correlated with intracellular ROS in alveolar macrophages, confirming that oxidative stress indicators of underground coal workers are correlated with the progression of CWP.

Summarising, extensive bibliography such as the results published in this work identify Fe and pyrite as potentially hazardous agents. They may promote oxidative stress and ROS and also could be involved in CWP injuries. In short, these components should be carefully monitored and controlled in coal mines due to their possible negative consequences.

Other transition metals, such as Ti, Cu, Ni, Mo, Co, Cr, and V may be agents in the formation and transformation of ROS (Aruoma, 1998; Lighty et al., 2000; Lloyd and Phillips, 1999; Shi et al., 1992; Shi and Dalal, 1992; Stohs and Bagchi, 1995; Strlič et al., 2003; Valko et al., 2005; Yu et al., 2020). Latvala et al. (2016) state the capability of Ni species to generate ROS. Moreno et al. (2019) suggest that redox-active elements, such as Cu, V and Cr, can contribute to ROS production; however, redox-inactive Pb can produce ROS by acting directly on cellular molecules. Yu et al. (2020) found that Mn, Cr, Ti, Fe, Cu, Zn, Ni, and Mo were correlated with ROS in non-small cell lung cancer cell lines. So, as previously indicated here, Cu, Ni, Mo, Co, Cr, Pb and V transition metals are related to OP and could develop ROS. In spite of the correlation of OP^{AA} with U, data on the OP of this metal was not found in the literature.

Moreover, sulphate, anatase and silica minerals results were linked to promoting ROS pathologies, as also indicated by the bibliography. Fang et al. (2017) also found a relevant correlation between sulphate contents in ambient PM and OP, and Gilmour et al. (2004), using other approaches, identified sulphate as an important factor of toxicity. Schins and Borm (1999) suggested that sulphate content in coal dust could play a dominant role in antiprotease inactivation. In addition, sulphate may also promote solubility, enhancing further the development of OP and ROS (Weber et al., 2016). Fubini and Hubbard (2003) reported in detail two main sources of ROS contributing to adverse reactions with silica: i) particle-generated free radicals and ROS (acting on cells); and ii) extracellular components and cell-generated ROS and reactive nitrogen species (RNS). Hamilton et al. (2009) demonstrated that anatase (TiO_2) could create an increase in toxic particles and produce an inflammatory response in lungs.

In addition to this, Zazouli et al. (2021) evaluated the cross correlation (r) between OP and PM_4 components from eight underground coal mines in Alborz Coal Basin. The results were in concordance with this study, with relatively high r values for elements such as Pb, Al, As, Cr or Co. Of special relevance are the similar results obtained for Fe in that and the present studies (r = 0.93 and 0.83, respectively).

3.2.4.2. Glutathione oxidative potential (OP^{GSH}). The moisture contents, and those of B and Na, are highly correlated with OP^{GSH} and, to a lesser degree, with the particle size, W and Ge. These associations could indirectly reflect the association of organic matter with OP^{GSH}. When an increase of coaly organic matter in dust occurs, the moisture content and the content of elements, typically associated with organic matter such as B, Ge and W (Swaine, 1990), also increase. Furthermore, the increase of organic matter in RD yields to a coarser particle size (Trechera et al., 2020, 2021). The association of organic matter-OP^{GSH} in these cases is probably related to specific patterns of radicals or organic components. Xu et al. (2017) demonstrate that the wettability of coal dust is closely related to the surface hydroxyl functional group, which, as previous commented, can contribute to the pathogenesis of CWP. This is relevant because moisture is an important parameter, among others, in defining

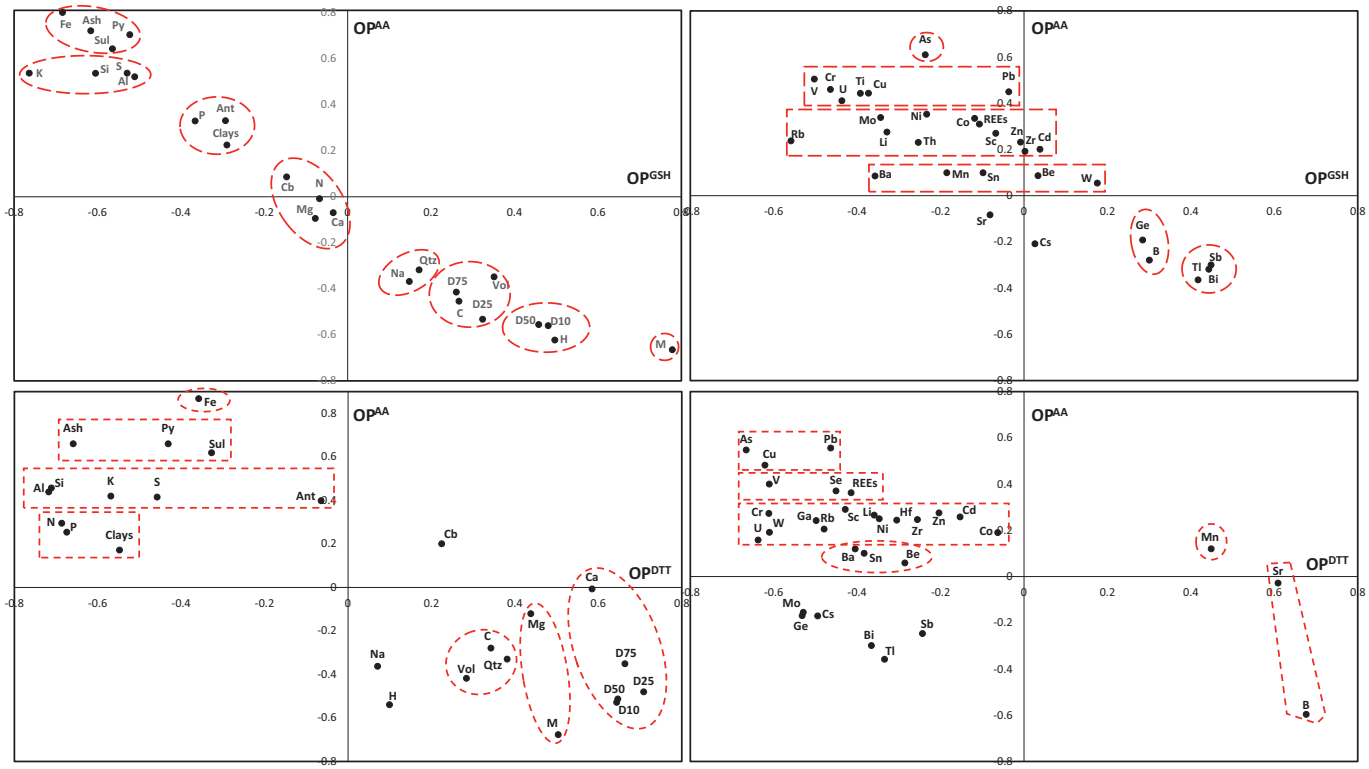

Fig. 4. Cross-correlation plots between the Pearson's correlation coefficients of geochemical parameters of all channel profile samples <4 μm (CP_4) (mineralogy, chemistry, size, and proximate analysis) from bituminous coals (12 of 22 samples) with their respective OP^{AA} vs OP^{GSH}, and OP^{AA} vs OP^{DTT}. Py, Pyrite; Ant, Anatase; Sul, Sulphates; Cb, Carbonates; Qtz, Quartz; D_{10}, D_{25}, D_{50}, D_{75}, percentiles 10, 25, 50 and 75 of the particle size in μm, respectively; Vol, Volatile Matter; M, Moisture.

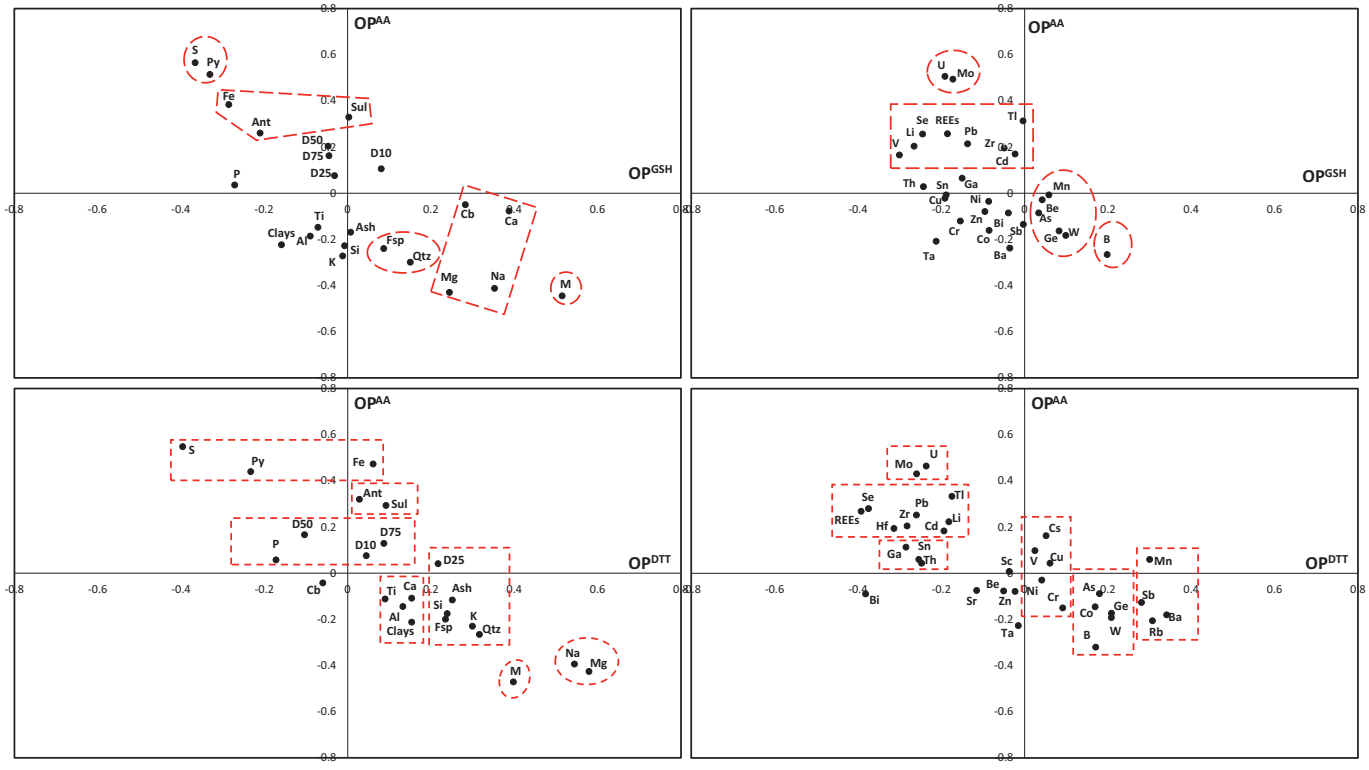

Fig. 5. Cross-correlation plots between the Pearson's correlation coefficients of geochemical parameters with their respective OP^{AA}, OP^{GSH}, and OP^{DTT}. All channel profile samples <4 μm (CP_4) and actual respirable coal mine dust samples showed in Table S4 are evaluated. Py, Pyrite; Ant, Anatase; Sul, Sulphates; Cb, Carbonates; Qtz, Quartz; Fsp, Feldspar; D_{10}, D_{25}, D_{50}, D_{75}, percentiles 10, 25, 50 and 75 of the particle size in μm, respectively; Vol, Volatile Matter; M, Moisture.

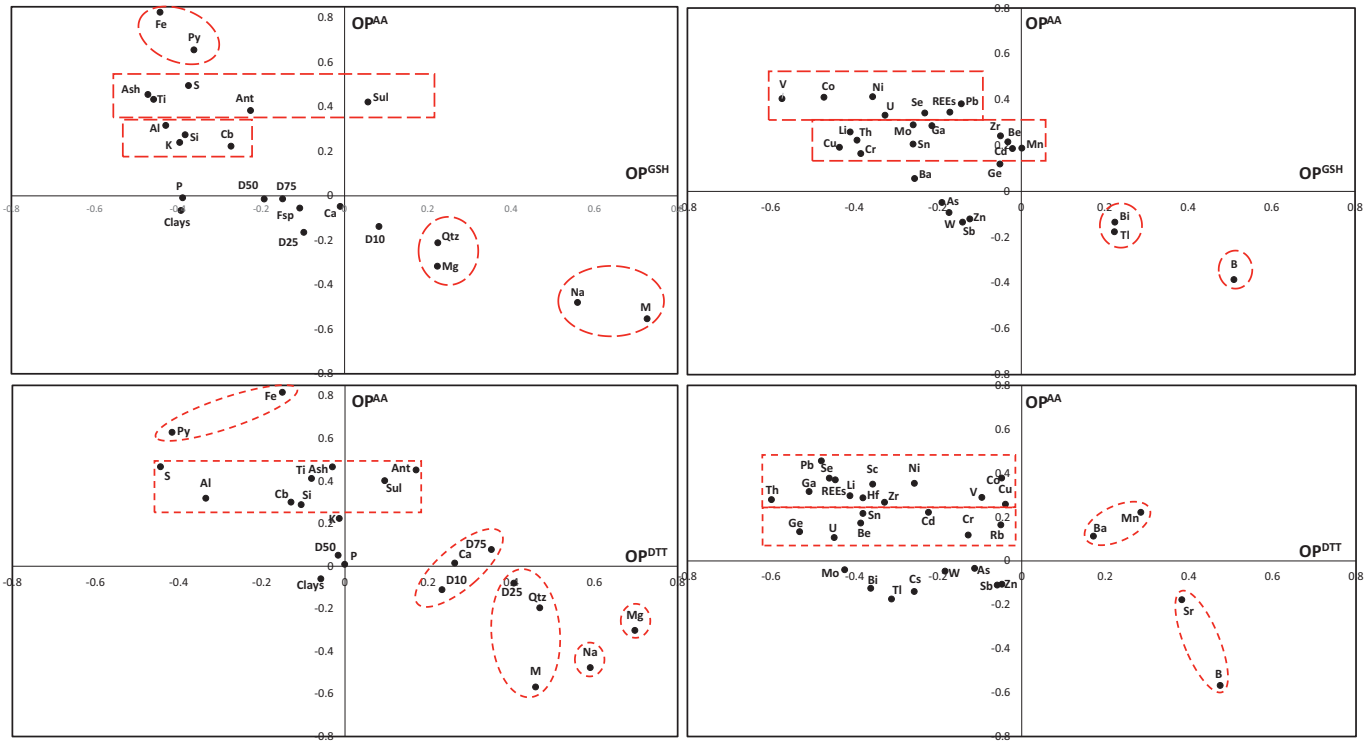

Fig. 6. Cross-correlation plots between the Pearson's correlation coefficients of geochemical parameters with their respective OP^{AA}, OP^{GSH}, and OP^{DTT}. Only the bituminous channel profile samples <4 μm (CP_4) and actual respirable coal mine dust samples showed in Table S4 are evaluated. Py, Pyrite; Ant, Anatase; Sul, Sulphates; Cb, Carbonates; Qtz, Quartz; Fsp, Feldspar; D_{10}, D_{25}, D_{50}, D_{75}, percentiles 10, 25, 50 and 75 of the particle size in μm, respectively; Vol, Volatile Matter; M, Moisture.

coal rank, decreasing as coal rank increases (Stach et al., 1982). However, Attfield and Morring (1992), Huang et al. (2005), Maclaren et al. (1989) and Huang et al. (1998) reported an increase of CWP with coal rank. The C content (% daf) in coal increases (by reducing H and O contents) as coal rank does (Stach et al., 1982), and this might increase specific surface and free radicals in the organic matrix, which could explain its higher cytotoxicity and pathogenicity (Castranova and Vallyathan, 2000; Dalal et al., 1995).

Furthermore, Pedroso-Fidelis et al. (2020) evaluated pulmonary oxidative stress in wild bats exposed to coal dust. They posited that, when Na concentration, among other metals, increased during coal dust exposure, an increased ROS was evident if compared with the control. Additionally, Alcala-Orozco et al. (2020) evidenced coal dust exposure generates a negative regulation in various genes, including GSH, which possibly develop oxidative stress. Moreover, Iram Batool et al. (2020) demonstrated that GSH levels are reduced in the coal miners with high exposure to coal dust, which reveals an elevated level of oxidative stress. They ordered in different levels the exposure of coal dust and the possible effect of workers (underground workers < surface workers < administrative group), supposing and recommending that workers with better health habits nutrition might cause an increase in antioxidant activity protecting the cell of the damage of the oxidative stress.

3.2.4.3. Dithiothreitol oxidative potential (OP^{DTT}). The main coal components showing correlation with OP^{DTT} in this study are Mg, B, moisture content and, to a lesser degree, particle size, quartz, Na, Ca, Mn, Sr, Ge, W, and Ba. As for OP^{GSH}, the results of correlation analysis for OP^{DTT} point to an association with the content of organic matter, as indicated by the correlation with moisture, B, W and Ge.

Furthermore, quartz, and carbonate minerals (traced by Ca, Mg, Sr, Mn) might also have an impact on OP^{DTT}. Mn was found to be associated with OP^{DTT} (Charrier and Anastasio, 2012; Cheng et al., 2021; Gao et al., 2020; Nishita-Hara et al., 2019; Yu et al., 2018). Nishita-Hara et al. (2019) demonstrated a correlation between Mg ($r = 0.56$) and Ba ($r = 0.61$) species with OP^{DTT} for PM from Asian dust events. Moreover, Gao et al. (2020) showed a correlation of Mg- and water insoluble-Mg and -Mn and water soluble-Ca with OP^{DTT}. No association has been identified in prior studies between quartz and OP^{DTT} as has been demonstrated in this study.

Finally, Barraza et al. (2020) found positive correlation between OP^{DTT} and Ba in the North Amazon Region in Ecuador, indicating that Ba is one of the main sources that is associated with ROS, after analysing the principals PM_{10} contributor of oil refining and industrial activities.

4. Conclusions and Recommendations

In this study, the respirable fraction (<4 μm, CP_4) from bulk powdered coal channel profile samples (CP) from various locations in China was obtained in the laboratory. The selection of coal samples was based on analysing a wide coverage of geochemical patterns (major and trace element contents and mineralogy) and coal ranks. As could be expected, CP_4/CP ratios for most elements and minerals were close to 1.0, with the exception of sulphate minerals, Fe, S, Mo, Ge, and Mn, with contents decreasing in CP_4 (CP_4/CP ratios between 0.6 and 0.8), and anatase, Na, Cs, W, Zn, and Zr, increasing in CP_4 (CP_4/CP ratios higher than 1.5).

Oxidative Potential (OP) tests, using Ascorbic Acid (AA) and Glutathione (GSH) as indicators, were performed for the CP_4 coals samples. The total OP ($OP^{TOT} = OP^{AA} + OP^{GSH}$) of CP_4 is relatively low (1.2%OP^{TOT}μg^{-1}) when compared with that reported for other particulate matter (PM), such as PM from subway systems (2.5%$OP^{TOT}\cdot\mu g^{-1}$), roadsides (3.6%$OP^{TOT}\cdot\mu g^{-1}$), or urban background pollution (1.5 to 4.0%$OP^{TOT}\cdot\mu g^{-1}$). The cross-correlation analysis shows that OP^{AA} is linked to specific inorganic components, whereas OP^{GSH} and dithiothreitol (OP^{DTT}) are related to organic components.

Furthermore, the OP correlation with specific components increases when the analysis is done for a specific coal rank (bituminous). Thus,

the correlation of Fe and pyrite with OP^{AA} reached r = 0.69 and 0.54, respectively, which increased to 0.80 and 0.70, respectively when only bituminous coals were considered. Moreover, their correlation remains, Fe (r = 0.83) and pyrite (r = 0.66) when only bituminous coals and coals dust are taken into account. This fact could demonstrate that bituminous coals contain more oxidising species of Fe and pyrite, which are more likely to generate reactive oxygen species (ROS) and are also transmitted to bituminous coal dust. However also that the scattering of the regression is smaller by reducing the potential effect of rank-related parameters on OP.

On the other hand, moisture content (as an indicator of the coaly organic matter content) is correlated with OP^{GSH} (r = 0.67), and these associations are stronger for bituminous coals (r = 0.78). Furthermore, moisture-OP^{GSH} correlation in bituminous coals and coal dust are also important, r = 0.73. This is the same with OP^{DTT} indicator, which shows an increased correlation with the parameters in bituminous coals for Mg and Na (ineffective in coal and bituminous coals), starting with low correlations of Mg (r = 0.31), increasing in bituminous coals, Mg (r = 0.44), and rising after bituminous coal and coal dust combinations, Mg (r = 0.70) and Na (r = 0.59).

To validate the method used (extraction of CP_4 to determine the OP of the derived respirable coal dust, RD) a correlation re-analysis was carried out by including actual RD and associated OP data from prior studies. This re-analysis conformed most of the results obtained for CP_4, especially when considering only bituminous coals. The results demonstrate that noticeable associations of Fe (r = 0.83) and pyrite (r = 0.66) are clearly linked with OP^{AA}. Organic matter, as identified by the parameters of moisture (r = 0.73), Na (r = 0.56) and B (r = 0.51) control OP^{GSH}, whereas Mg (r = 0.70) and Na (r = 0.59) are associated with OP^{DTT}.

A multilinear regression analysis allowed the geochemical associations with OP to be categorised. The results indicate that Fe, pyrite and sulphate minerals (indicating acidic species from pyrite oxidation) showing high correlation with elevated r (0.8–0.9), followed by anatase, and in a much lower proportion U, Mo, V and Pb, clearly govern the OP^{AA} of CP_4 and RD; while the contents of organic matter (traced by those of moisture, B and the coarse size, r = 0.85–0.75), Ca, carbonate minerals control OP^{GSH}; and those of Mg, Na, quartz, organic matter and Ba regulate OP^{DTT}, with r coefficients approximate to 0.7.

The results support the conclusions drawn from Harrington et al. (2012) and Huang et al. (2005) concerning the relevance of the Fe and pyrite contents in inhalable particles from coal dust ability to lead to oxidative stress, which, in turn, may lead to lung injury and coal workers' pneumoconiosis (CWP) development. Moreover, correlations obtained are in concordance with other similar studies (Zazouli et al., 2021). The results also show that the organic matter of coal can increase OP^{DTT} and OP^{GSH}. Thus, the results highlight the need to implement high efficiency primary and secondary coal dust abatement measures in coal mines, especially in the mining of high pyrite coals. As intensive coal mining in China will continue in the forthcoming decades and because the production has increased dramatically since 2000, a large number of miners are exposed to coal dust, and research on coal dust and occupational health and on coal dust abatement controls should be continuously supported.

Credit authorship contribution statement

The corresponding author, Pedro Trechera, is responsible for ensuring that the descriptions are accurate and agreed by all authors, participated in sampling, did analyses and writing.

Teresa Moreno discussed results, wrote some sections and reviewed manuscript.

Natalia Moreno did DRX analyses, discussed results and reviewed manuscript.

Joaquim Cortés did some chemical and separation analysis, discussed results and reviewed manuscript.

Fulvio Amato reviewed manuscript.

Zhuang Xinguo, Baoqing Li, Jing Li, Yunfei Shangguan and Patricia Córdoba, participated in sampling, discussed results and reviewed manuscript.

Ana Oliete and Frank Kelly did some OP analysis, wrote a section and reviewed manuscript.

Takoua Mhadhbi, Jean Luc Jaffrezo and Gaelle Uzu did some OP analysis, wrote a section and reviewed manuscript.

Xavier Querol participated in sampling, did some analysis, discussed results, wrote some sections and reviewed the manuscript.

Declaration of competing interest

The authors declare that they have no known competing financial interests or personal relationships that could have appeared to influence the work reported in this paper.

Acknowledgments

This study was supported by Generalitat de Catalunya (AGAUR 2017 SGR41), Spain; by the National Science Foundation of China (grant 41972180); the Program of Introducing Talents of Discipline to Universities (grant B14031) and Overseas Top Scholars Program for the Recruitment of Global Experts, China; and by the Spanish Ministry of Science and Innovation (Excelencia Severo Ochoa, Project CEX2018-000794-S). Malvern Mastersizer Scirocco 2000 extension measurements were performed at the ICTS NANBIOSIS by the Nanostructured Liquids Unit (U12) of the CIBER in Bioengineering, Biomaterials & Nanomedicine (CIBER-BBN), located at the IQAC-CSIC (Barcelona, Spain). Pedro Trechera is contracted by the ROCD (Reducing risks from Occupational exposure to Coal Dust) project supported by the European Commission Research Fund for Coal and Steel; Grant Agreement Number 754205.

Appendix A. Supplementary data

Supplementary data to this article can be found online at https://doi.org/10.1016/j.scitotenv.2021.149486.

References

Ahamed, M.A.A., Perera, M.S.A., Matthai, S.K., Ranjith, P.G., Dong-yin, L., 2019. Coal composition and structural variation with rank and its influence on the coal-moisture interactions under coal seam temperature conditions – a review article. J. Pet. Sci. Eng. https://doi.org/10.1016/j.petrol.2019.06.007.

Alcala-Orozco, M., Caballero-Gallardo, K., Olivero-Verbel, J., 2020. Intergenerational effects of coal dust on Tribolium castaneum. Herbst. Environ. Res. 182, 109055. https://doi.org/10.1016/j.envres.2019.109055.

Allardice, D.J., Clemow, L.M., Jackson, W.R., 2003. Determination of the acid distribution and total acidity of low-rank coals and coal-derived materials by an improved barium exchange technique. Fuel 82, 35–40. https://doi.org/10.1016/S0016-2361(02)00193-X.

Aruoma, O.I., 1998. Free radicals, oxidative stress, and antioxidants in human health and disease. J. Am. Oil Chem. Soc. 75, 199–212. https://doi.org/10.1007/s11746-998-0032-9.

Attfield, M.D., Morring, K., 1992. An investigation into the relationship between coal workers' pneumoconiosis and dust exposure in U.S. coal miners. Am. Ind. Hyg. Assoc. J. 53, 486–492. https://doi.org/10.1080/15298669291360012.

Ávila Júnior, S., Possamai, F.P., Budni, P., Backes, P., Parisotto, E.B., Rizelio, V.M., Torres, M.A., Colepicolo, P., Wilhelm Filho, D., 2009. Occupational airborne contamination in South Brazil: 1. oxidative stress detected in the blood of coal miners. Ecotoxicology 18, 1150–1157. https://doi.org/10.1007/s10646-009-0364-8.

Ayres, J.G., Borm, P., Cassee, F.R., Castranova, V., Donaldson, K., Ghio, A., Harrison, R.M., Hider, R., Kelly, F., Kooter, I.M., Marano, F., Maynard, R.L., Mudway, I., Nel, A., Sioutas, C., Smith, S., Baeza-Squiban, A., Cho, A., Duggan, S., Froines, J., 2008. Evaluating the toxicity of airborne particulate matter and nanoparticles by measuring oxidative stress potential - A workshop report and consensus statement. Inhalation Toxicology. Taylor & Francis, pp. 75–99 https://doi.org/10.1080/08958370701665517.

Baker, M.A., Cerniglia, G.J., Zaman, A., 1990. Microtiter plate assay for the measurement of glutathione and glutathione disulfide in large numbers of biological samples. Anal. Biochem. 190, 360–365. https://doi.org/10.1016/0003-2697(90)90208-Q.

Barraza, F., Uzu, G., Jaffrezo, J.-L., Schreck, E., Budzinski, H., Le Menach, K., Dévier, M.-H., Guyard, H., Calas, A., Perez, M.-I., Villacreces, L.-A., Maurice, L., 2020. Contrasts in chemical composition and oxidative potential in PM10 near flares in oil extraction

and refining areas in Ecuador. Atmos. Environ. 223, 117302. https://doi.org/10.1016/j.atmosenv.2020.117302.
Borm, P.J.A., Kelly, F., Künzli, N., Schins, R.P.F., Donaldson, K., 2007. Oxidant generation by particulate matter: from biologically effective dose to a promising, novel metric. Occup. Environ. Med. https://doi.org/10.1136/oem.2006.029090.
BP, 2020. BP Statistical Review of World Energy 2020.
Brown, J.S., Gordon, T., Price, O., Asgharian, B., 2013. Thoracic and respirable particle definitions for human health risk assessment. Part. Fibre Toxicol. 10, 12. https://doi.org/10.1186/1743-8977-10-12.
Calas, A., Uzu, G., Kelly, F.J., Houdier, S., Martins, J.M.F., Thomas, F., Molton, F., Charron, A., Dunster, C., Oliete, A., Jacob, V., Besombes, J.-L., Chevrier, F., Jaffrezo, J.-L., 2018. Comparison between five acellular oxidative potential measurement assays performed with detailed chemistry on PM₁₀ samples from the city of Chamonix (France). Atmos. Chem. Phys. 18, 7863–7875. https://doi.org/10.5194/acp-18-7863-2018.
Castranova, V., 2000. From coal mine dust to quartz: mechanisms of pulmonary pathogenicity. Inhal. Toxicol. 12, 7–14. https://doi.org/10.1080/08958378.2000.11463226.
Castranova, V., Vallyathan, V., 2000. Silicosis and coal workers' pneumoconiosis. Environ. Health Perspect. 108, 675–684. https://doi.org/10.1289/ehp.00108s4675.
Charrier, J.G., Anastasio, C., 2012. On dithiothreitol (DTT) as a measure of oxidative potential for ambient particles: evidence for the importance of soluble \newline transition metals. Atmos. Chem. Phys. 12, 9321–9333. https://doi.org/10.5194/acp-12-9321-2012.
Chen, H., Feng, Q., Long, R., Qi, H., 2013. Focusing on coal miners' occupational disease issues: a comparative analysis between China and the United States. Saf. Sci. 51, 217–222. https://doi.org/10.1016/j.ssci.2012.06.025.
Cheng, Y., Ma, Y., Dong, B., Qiu, X., Hu, D., 2021. Pollutants from primary sources dominate the oxidative potential of water-soluble PM2.5 in Hong Kong in terms of dithiothreitol (DTT) consumption and hydroxyl radical production. J. Hazard. Mater. 405, 124218. https://doi.org/10.1016/j.jhazmat.2020.124218.
Choi, H., Thiruppathiraja, C., Kim, S., Rhim, Y., Lim, J., Lee, S., 2011. Moisture readsorption and low temperature oxidation characteristics of upgraded low rank coal. Fuel Process. Technol. 92, 2005–2010. https://doi.org/10.1016/j.fuproc.2011.05.025.
Christian, R.T., Nelson, J.B., Cody, T.E., Larson, E., Bingham, E., 1979. Coal workers' pneumoconiosis: in vitro study of the chemical composition and particle size as causes of the toxic effects of coal. Environ. Res. 20, 358–365. https://doi.org/10.1016/0013-9351(79)90012-4.
Chung, F.H., 1974. Quantitative interpretation of X-ray diffraction patterns of mixtures. I. Matrix-flushing method for quantitative multicomponent analysis. J. Appl. Crystallogr. 7, 519–525. https://doi.org/10.1107/s0021889874010375.
Cohn, C.A., Laffers, R., Schoonen, M.A.A., 2006a. Using yeast RNA as a probe for generation of hydroxyl radicals by earth materials. Environ. Sci. Technol. 40, 2838–2843. https://doi.org/10.1021/es052301k.
Cohn, C.A., Laffers, R., Simon, S.R., O'riordan, T., Schoonen, M.A., 2006b. Role of Pyrite in Formation of Hydroxyl Radicals in Coal: Possible Implications for Human Health. https://doi.org/10.1186/1743-8977-3-16.
Daellenbach, K.R., Uzu, G., Jiang, J., Cassagnes, L.E., Leni, Z., Vlachou, A., Stefenelli, G., Canonaco, F., Weber, S., Segers, A., Kuenen, J.J.P., Schaap, M., Favez, O., Albinet, A., Aksoyoglu, S., Dommen, J., Baltensperger, U., Geiser, M., El Haddad, I., Jaffrezo, J.L., Prévôt, A.S.H., 2020. Sources of particulate-matter air pollution and its oxidative potential in Europe. Nature 587, 414–419. https://doi.org/10.1038/s41586-020-2902-8.
Dai, S., Ren, D., Hou, X., Shao, L., 2003. Geochemical and mineralogical anomalies of the late Permian coal in the Zhijin coalfield of Southwest China and their volcanic origin. Int. J. Coal Geol. 55, 117–138. https://doi.org/10.1016/S0166-5162(03)00083-1.
Dai, S.F., Zhou, Y.P., Ren, D.Y., Wang, X.B., Li, D., Zhao, L., 2007. Geochemistry and mineralogy of the Late Permian coals from the Songzo Coalfield, Chongqing, southwestern China. Sci. China Ser. D Earth Sci. 50, 678–688. https://doi.org/10.1007/s11430-007-0001-4.
Dai, S., Ren, D., Zhou, Y., Chou, C.L., Wang, X., Zhao, L., Zhu, X., 2008. Mineralogy and geochemistry of a superhigh-organic-sulfur coal, Yanshan Coalfield, Yunnan, China: evidence for a volcanic ash component and influence by submarine exhalation. Chem. Geol. 255, 182–194. https://doi.org/10.1016/j.chemgeo.2008.06.030.
Dai, S., Wang, X., Chen, W., Li, D., Chou, C.L., Zhou, Y., Zhu, C., Li, H., Zhu, X., Xing, Y., Zhang, W., Zou, J., 2010. A high-pyrite semianthracite of Late Permian age in the Songzao Coalfield, southwestern China: mineralogical and geochemical relations with underlying mafic tuffs. Int. J. Coal Geol. 83, 430–445. https://doi.org/10.1016/j.coal.2010.06.004.
Dai, S., Jiang, Y., Ward, C.R., Gu, L., Seredin, V.V., Liu, H., Zhou, D., Wang, X., Sun, Y., Zou, J., Ren, D., 2012. Mineralogical and geochemical compositions of the coal in the guanbanwusu mine, Inner Mongolia, China: further evidence for the existence of an Al (Ga and REE) ore deposit in the jungar coalfield. Int. J. Coal Geol. 98, 10–40. https://doi.org/10.1016/j.coal.2012.03.003.
Dai, S., Graham, I.T., Ward, C.R., 2016. A review of anomalous rare earth elements and yttrium in coal. Int. J. Coal Geol. 159, 82–95. https://doi.org/10.1016/j.coal.2016.04.005.
Dalal, N.S., Newman, J., Pack, D., Leonard, S., Vallyathan, V., 1995. Hydroxyl radical generation by coal mine dust: possible implication to coal workers' pneumoconiosis (CWP). Free Radic. Biol. Med. 18, 11–20. https://doi.org/10.1016/0891-5849(94)E0094-Y.
Dodson, J., Li, X., Sun, N., Atahan, P., Zhou, X., Liu, H., Zhao, K., Hu, S., Yang, Z., 2014. Use of coal in the Bronze Age in China. The Holocene 24, 525–530. https://doi.org/10.1177/0959683614523155.
Du, F., Qiao, J., Zhao, X., Tan, F., Li, C., Luo, Z., 2021. Enrichment of V in Late Permian coals in Gemudi Mine, Western Guizhou, SW China. J. Geochem. Explor. 221, 106701. https://doi.org/10.1016/j.gexplo.2020.106701.
European Committee for Standardization, 1992. Workplace Atmospheres: Size Fraction Definitions for Measurement of Airborne Particles in the Workplace, CEN - EN 481.
Fan, Y., Xia, Y., 2012. Exploring energy consumption and demand in China. Energy 40, 23–30. https://doi.org/10.1016/j.energy.2011.09.049.
Fan, Z., Xu, F., 2021. Health risks of occupational exposure to toxic chemicals in coal mine workplaces based on risk assessment mathematical model based on deep learning. Environ. Technol. Innov. 22, 101500. https://doi.org/10.1016/j.eti.2021.101500.
Fang, T., Guo, H., Zeng, L., Verma, V., Nenes, A., Weber, R.J., 2017. Highly acidic ambient particles, soluble metals, and oxidative potential: a link between sulfate and aerosol toxicity. Environ. Sci. Technol. 51, 40. https://doi.org/10.1021/acs.est.6b06151.
Fang, T., Lakey, P.S.J., Weber, R.J., Shiraiwa, M., 2019. Oxidative potential of particulate matter and generation of reactive oxygen species in epithelial lining fluid. Environ. Sci. Technol. 53, 12784–12792. https://doi.org/10.1021/acs.est.9b03823.
Finkelman, R.B., Orem, W., Castranova, V., Tatu, C.A., Belkin, H.E., Zheng, B., Lerch, H.E., Maharaj, S.V., Bates, A.L., 2002. Health impacts of coal and coal use: possible solutions. Int. J. Coal Geol. 50, 425–443. https://doi.org/10.1016/S0166-5162(02)00125-8.
Fu, P.P., Xia, Q., Hwang, H.M., Ray, P.C., Yu, H., 2014. Mechanisms of nanotoxicity: generation of reactive oxygen species. J. Food Drug Anal. 22, 64–75. https://doi.org/10.1016/j.jfda.2014.01.005.
Fubini, B., Hubbard, A., 2003. Reactive oxygen species (ROS) and reactive nitrogen species (RNS) generation by silica in inflammation and fibrosis. Free Radic. Biol. Med. https://doi.org/10.1016/S0891-5849(03)00149-7.
Gao, D., Mulholland, J.A., Russell, A.G., Weber, R.J., 2020. Characterization of water-insoluble oxidative potential of PM2.5 using the dithiothreitol assay. Atmos. Environ. 224, 117327. https://doi.org/10.1016/j.atmosenv.2020.117327.
Gelegdorj, E., Chunag, A., Gordon, R.B., Park, J.S., 2007. Transitions in cast iron technology of the nomads in Mongolia. J. Archaeol. Sci. 34, 1187–1196. https://doi.org/10.1016/j.jas.2006.10.007.
Gilmour, M.I., O'Connor, S., Dick, C.A.J., Miller, C.A., Linak, W.P., 2004. Differential pulmonary inflammation and in vitro cytotoxicity of size-fractionated fly ash particles from pulverized coal combustion. J. Air Waste Manage. Assoc. 54, 286–295. https://doi.org/10.1080/10473289.2004.10470906.
Godri, K.J., Harrison, R.M., Evans, T., Baker, T., Dunster, C., Mudway, I.S., Kelly, F.J., 2011. Increased oxidative burden associated with traffic component of ambient particulate matter at roadside and urban background schools sites in London. PLoS One 6, e21961. https://doi.org/10.1371/journal.pone.0021961.
Guo, J., Yao, D., Chen, P., Chen, J., Shi, F., 2017. Distribution, enrichment and modes of occurrence of arsenic in Chinese coals. Minerals 7. https://doi.org/10.3390/min7070114.
Hamilton, R.F., Wu, N., Porter, D., Buford, M., Wolfarth, M., Holian, A., 2009. Particle length-dependent titanium dioxide nanomaterials toxicity and bioactivity. Part. Fibre Toxicol. 6, 1–11. https://doi.org/10.1186/1743-8977-6-35.
Han, S., Chen, H., Long, R., Cui, X., 2018. Peak coal in China: a literature review. Resour. Conserv. Recycl. 129, 293–306. https://doi.org/10.1016/j.resconrec.2016.08.012.
Harrington, A.D., Hylton, S., Schoonen, M.A.A., 2012. Pyrite-driven reactive oxygen species formation in simulated lung fluid: implications for coal workers' pneumoconiosis. Environ. Geochem. Health 34, 527–538. https://doi.org/10.1007/s10653-011-9438-7.
Huang, X., Finkelman, R.B., 2008. Understanding the chemical properties of macerals and minerals in coal and its potential application for occupational lung disease prevention. J. Toxicol. Environ. Health - Part B Crit. Rev. https://doi.org/10.1080/10937400701600552.
Huang, X., Fournier, J., Koenig, K., Chen, L.C., 1998. Content: Possible Role in Coal Workers' Pneumoconiosis, pp. 722–729.
Huang, C., Li, J., Zhang, Q., Huang, X., 2002. Role of bioavailable iron in coal dust-induced activation of activator protein-1 and nuclear factor of activated T cells: difference between Pennsylvania and Utah coal dusts. Am. J. Respir. Cell Mol. Biol. 27, 568–574. https://doi.org/10.1165/rcmb.4821.
Huang, X., Li, W., Attfield, M.D., Nádas, A., Frenkel, K., Finkelman, R.B., 2005. Mapping and prediction of coal workers' pneumoconiosis with bioavailable iron content in the bituminous coals. Environ. Health Perspect. 113, 964–968. https://doi.org/10.1289/ehp.7679.
IEA, 2020. World Energy Outlook 2020. IEA, Paris, p. 124.
Imai, Y., Kuba, K., Neely, G.G., Yaghubian-Malhami, R., Perkmann, T., van Loo, G., Ermolaeva, M., Veldhuizen, R., Leung, Y.H.C., Wang, H., Liu, H., Sun, Y., Pasparakis, M., Kopf, M., Mech, C., Bavari, S., Peiris, J.S.M., Slutsky, A.S., Akira, S., Hultqvist, M., Holmdahl, R., Nicholls, J., Jiang, C., Binder, C.J., Penninger, J.M., 2008. Identification of oxidative stress and toll-like receptor 4 signaling as a key pathway of acute lung injury. Cell 133, 235–249. https://doi.org/10.1016/j.cell.2008.02.043.
Iram Batool, A., Huma Naveed, N., Aslam, M., da Silva, J., Rehman, M., 2020. Coal Dust-induced Systematic Hypoxia and Redox Imbalance Among Coal Mine Workers. https://doi.org/10.1021/acsomega.0c03977.
Iriyama, K., Yoshiura, M., Iwamoto, T., Ozaki, Y., 1984. Simultaneous determination of uric and ascorbic acids in human serum by reversed-phase high-performance liquid chromatography with electrochemical detection. Anal. Biochem. 141, 238–243. https://doi.org/10.1016/0003-2697(84)90451-2.
Ishtiaq, M., Jehan, N., Khan, S.A., Muhammad, S., Saddique, U., Iftikhar, B., Zahidullah, 2018. Potential harmful elements in coal dust and human health risk assessment near the mining areas in Cherat, Pakistan. Environ. Sci. Pollut. Res. 25, 14666–14673. https://doi.org/10.1007/s11356-018-1655-5.
Izquierdo, M., Querol, X., 2012. Leaching behaviour of elements from coal combustion fly ash: an overview. Int. J. Coal Geol. https://doi.org/10.1016/j.coal.2011.10.006.
Janssen, N.A.H., Yang, A., Strak, M., Steenhof, M., Hellack, B., Gerlofs-Nijland, M.E., Kuhlbusch, T., Kelly, F., Harrison, R., Brunekreef, B., Hoek, G., Cassee, F., 2014. Oxidative potential of particulate matter collected at sites with different source characteristics. Sci. Total Environ. 472, 572–581. https://doi.org/10.1016/j.scitotenv.2013.11.099.

Jie, D., Xu, X., Guo, F., 2020. The future of coal supply in China based on non-fossil energy development and carbon price strategies. Energy 220, 119644. https://doi.org/10.1016/j.energy.2020.119644.
Kelly, F.J., 2003. Oxidative stress: its role in air pollution and adverse health effects. Occup. Environ. Med. 60, 612–616. https://doi.org/10.1136/oem.60.8.612.
Kim, Y.H., Warren, S.H., Krantz, Q.T., King, C., Jaskot, R., Preston, W.T., George, B.J., Hays, M.D., Landis, M.S., Higuchi, M., DeMarini, D.M., Gilmour, M.I., 2018. Mutagenicity and lung toxicity of smoldering vs. flaming emissions from various biomass fuels: implications for health effects from wildland fires. Environ. Health Perspect. 126, 017011. https://doi.org/10.1289/EHP2200.
Landen, D.D., Wassell, J.T., McWilliams, L., Patel, A., 2011. Coal dust exposure and mortality from ischemic heart disease among a cohort of U.S. coal miners. Am. J. Ind. Med. 54, 727–733. https://doi.org/10.1002/ajim.20986.
Lashgari, A., Kecojevic, V., 2016. Comparative analysis of dust emission of digging and loading equipment in surface coal mining. Int. J. Mining Reclam. Environ. 30, 181–196. https://doi.org/10.1080/17480930.2015.1028516.
Latvala, S., Hedberg, J., Bucchianico, S.Di, Möller, L., Odnevall Wallinder, I., Elihn, K., Karlsson, H.L., 2016. Nickel Release, ROS Generation and Toxicity of Ni and NiO Micro-and Nanoparticles. https://doi.org/10.1371/journal.pone.0159684.
Leni, Z., Cassagnes, L.E., Daellenbach, K.R., Haddad, I.El, Vlachou, A., Uzu, G., Prévôt, A.S.H., Jaffrezo, J.L., Baumlin, N., Salathe, M., Baltensperger, U., Dommen, J., Geiser, M., 2020. Oxidative stress-induced inflammation in susceptible airways by anthropogenic aerosol. PLoS One 15, 1–17. https://doi.org/10.1371/journal.pone.0233425.
Li, W., Lu, D., 1995. Industrial Geography of China.
Li, J., Zhuang, X., Querol, X., 2011. Trace element affinities in two high-Ge coals from China. Fuel 90, 240–247. https://doi.org/10.1016/j.fuel.2010.08.011.
Li, J., Zhuang, X., Querol, X., Font, O., Moreno, N., Zhou, J., Lei, G., 2012. High quality of Jurassic coals in the Southern and Eastern Junggar Coalfields, Xinjiang, NW China: geochemical and mineralogical characteristics. Int. J. Coal Geol. 99, 1–15. https://doi.org/10.1016/j.coal.2012.05.003.
Li, B., Zhuang, X., Li, J., Zhao, S., 2014. Geological controls on coal quality of the Yili Basin, Xinjiang, Northwest China. Int. J. Coal Geol. 131, 186–199. https://doi.org/10.1016/j.coal.2014.06.013.
Li, B., Zhuang, X., Li, J., Querol, X., Font, O., Moreno, N., 2016. Geological controls on mineralogy and geochemistry of the Late Permian coals in the Liulong Mine of the Liuzhi Coalfield, Guizhou Province, Southwest China. Int. J. Coal Geol. 154–155, 1–15. https://doi.org/10.1016/j.coal.2015.12.003.
Li, J., Zhuang, X., Yuan, W., Liu, B., Querol, X., Font, O., Moreno, N., Li, Jianfu, Gang, T., Liang, G., 2016. Mineral composition and geochemical characteristics of the Li-Ga-rich coals in the Buertaohai-Tianjiashipan mining district, Jungar Coalfield, Inner Mongolia. Int. J. Coal Geol. 167, 157–175. https://doi.org/10.1016/j.coal.2016.09.018.
Li, B., Zhuang, X., Li, J., Querol, X., Font, O., Moreno, N., 2017. Enrichment and distribution of elements in the Late Permian coals from the Zhina Coalfield, Guizhou Province, Southwest China. Int. J. Coal Geol. 171, 111–129. https://doi.org/10.1016/j.coal.2017.01.003.
Li, B., Zhuang, X., Querol, X., Li, J., Moreno, N., Córdoba, P., Shangguan, Y., Zhou, J., Ma, X., Liu, S., 2019a. Geological controls on enrichment of Mn, Nb (Ta), Zr (Hf), and REY within the Early Permian coals of the Jimunai Depression, Xinjiang Province, NW China. Int. J. Coal Geol. 215, 103298. https://doi.org/10.1016/j.coal.2019.103298.
Li, B., Zhuang, X., Querol, X., Moreno, N., Yang, L., Shangguan, Y., Li, J., 2019b. Mineralogy and geochemistry of Late Permian coals within the Tongzi Coalfield in Guizhou Province, Southwest China. Minerals 10, 44. https://doi.org/10.3390/min10010044.
Li, J., Xie, C., Long, H., 2019. The roles of inter-fuel substitution and inter-market contagion in driving energy prices: evidences from China's coal market. Energy Econ. 84, 104525. https://doi.org/10.1016/j.eneco.2019.104525.
Li, B., Zhuang, X., Querol, X., Moreno, N., Córdoba, P., Shangguan, Y., Yang, L., Li, J., Zhang, F., 2020. Geological controls on the distribution of REY-Zr (Hf)-Nb (Ta) enrichment horizons in late Permian coals from the Qiandongbei Coalfield, Guizhou Province, SW China. Int. J. Coal Geol. 231, 103604. https://doi.org/10.1016/j.coal.2020.103604.
Li, J., Wu, P., Yang, G., Pan, L., Zhuang, X., Querol, X., Moreno, N., Li, B., Shangguan, Y., 2020. Enrichment of Li–Ga–Zr–Hf and Se–Mo–Cr–V–As–Pb assemblages in the No. 11 superhigh organic sulfur coal from the Sangshuping Coal Mine, Weibei Coalfield, Shaanxi, North China. Energies 13, 6660. https://doi.org/10.3390/en13246660.
Li, B., Liu, G., Bi, M.S., Li, Z.B., Han, B., Shu, C.M., 2021. Self-ignition risk classification for coal dust layers of three coal types on a hot surface. Energy 216, 119197. https://doi.org/10.1016/j.energy.2020.119197.
Lighty, J.S., Veranth, J.M., Sarofim, A.F., 2000. Combustion aerosols: factors governing their size and composition and implications to human health. J. Air Waste Manage. Assoc. 50, 1565–1618. https://doi.org/10.1080/10473289.2000.10464197.
Lin, B., Tan, R., 2017. Estimating energy conservation potential in China's energy intensive industries with rebound effect. J. Clean. Prod. 156, 899–910. https://doi.org/10.1016/j.jclepro.2017.04.100.
Liu, T., Liu, S., 2020. The impacts of coal dust on miners' health: a review. Environ. Res. https://doi.org/10.1016/j.envres.2020.109849.
Liu, R., Zhou, G., Wang, C., Jiang, W., Wei, X., 2020. Preparation and performance characteristics of an environmentally-friendly agglomerant to improve the dry dust removal effect for filter material. J. Hazard. Mater. 397, 122734. https://doi.org/10.1016/j.jhazmat.2020.122734.
Liu, J., Spiro, B.F., Dai, S., French, D., Graham, I.T., Wang, X., Zhao, L., Zhao, J., Zeng, R., 2021. Strontium isotopes in high- and low-Ge coals from the Shengli Coalfield, Inner Mongolia, northern China: new indicators for Ge source. Int. J. Coal Geol. 233, 103642. https://doi.org/10.1016/j.coal.2020.103642.
Lloyd, D.R., Phillips, D.H., 1999. Oxidative DNA damage mediated by copper(II), iron(II) and nickel(II) Fenton reactions: evidence for site-specific mechanisms in the formation of double-strand breaks, 8-hydroxydeoxyguanosine and putative intrastrand cross-links. Mutat. Res. - Fundam. Mol. Mech. Mutagen. 424, 23–36. https://doi.org/10.1016/S0027-5107(99)00005-6.
Ma, D., Qin, B., Gao, Y., Jiang, J., Feng, B., 2020. Study on the explosion characteristics of methane–air with coal dust originating from low-temperature oxidation of coal. Fuel 260, 116304. https://doi.org/10.1016/j.fuel.2019.116304.
Maclaren, W.M., Hurley, J.F., Collins, P.R., Cowie, A.J., 1989. Factors associated with the development of progressive massive fibrosis in British coalminers: a case-control study. Br. J. Ind. Med. 46, 597–607. https://doi.org/10.1136/oem.46.9.597.
MacNee, W., 2001. Oxidative stress and lung inflammation in airways disease. Eur. J. Pharmacol. https://doi.org/10.1016/S0014-2999(01)01320-6.
Mao, J.X., Tong, H.L., 2013. Coal resources, production and use in China. The Coal Handbook: Towards Cleaner Production. Elsevier Inc., pp. 220–234 https://doi.org/10.1533/9781782421177.2.220.
Masto, R.E., George, J., Rout, T.K., Ram, L.C., 2017. Multi element exposure risk from soil and dust in a coal industrial area. J. Geochem. Explor. 176, 100–107. https://doi.org/10.1016/j.gexplo.2015.12.009.
McCunney, R.J., Morfeld, P., Payne, S., 2009. What component of coal causes coal workers' pneumoconiosis? J. Occup. Environ. Med. 51, 462–471. https://doi.org/10.1097/JOM.0b013e3181a01ada.
Mo, J., Wang, L., Au, W., Su, M., 2014. Prevalence of coal workers' pneumoconiosis in China: a systematic analysis of 2001-2011 studies. Int. J. Hyg. Environ. Health https://doi.org/10.1016/j.ijheh.2013.03.006.
Moreno, T., Amato, F., Querol, X., Alastuey, A., Gibbons, W., 2008. Trace element fractionation processes in resuspended mineral aerosols extracted from australian continental surface materials. Soil Res. 46, 128. https://doi.org/10.1071/SR07121.
Moreno, T., Kelly, F.J., Dunster, C., Oliete, A., Martins, V., Reche, C., Minguillón, M.C., Amato, F., Capdevila, M., de Miguel, E., Querol, X., 2017. Oxidative potential of subway PM2.5. Atmos. Environ. 148, 230–238. https://doi.org/10.1016/j.atmosenv.2016.10.045.
Moreno, T., Trechera, P., Querol, X., Lah, R., Johnson, D., Wrana, A., Williamson, B., 2019. Trace element fractionation between PM10 and PM2.5 in coal mine dust: implications for occupational respiratory health. Int. J. Coal Geol. 203, 52–59. https://doi.org/10.1016/j.coal.2019.01.006.
Munir, M.A.M., Liu, G., Yousaf, B., Ali, M.U., Abbas, Q., Ullah, H., 2018. Enrichment of Bi-Be-Mo-Cd-Pb-Nb-Ga, REEs and Y in the Permian coals of the Huainan Coalfield, Anhui China. Ore Geol. Rev. 95, 431–455. https://doi.org/10.1016/j.oregeorev.2018.02.037.
Murphy, R., Strongin, D.R., 2009. Surface reactivity of pyrite and related sulfides. Surf. Sci. Rep. https://doi.org/10.1016/j.surfrep.2008.09.002.
Nardi, J., Nascimento, S., Göethel, G., Gauer, B., Sauer, E., Fão, N., Cestonaro, L., Peruzzi, C., Souza, J., Garcia, S.C., 2018. Inflammatory and oxidative stress parameters as potential early biomarkers for silicosis. Clin. Chim. Acta https://doi.org/10.1016/j.cca.2018.05.045.
NIOSH, 2002. Health Effects of Occupational Exposure to Respirable Crystalline Silica. Department of Health and Human Services, Centers for Disease Control and Prevention, National Institute for Occupational Safety and Health doi:2002-129.
Nishita-Hara, C., Hirabayashi, M., Hara, K., Yamazaki, A., Hayashi, M., 2019. Dithiothreitol-measured oxidative potential of size-segregated particulate matter in Fukuoka, Japan: effects of asian dust events. GeoHealth 3, 160–173. https://doi.org/10.1029/2019GH000189.
Pedroso-Fidelis, G. dos S., Farias, H.R., Mastella, G.A., Boufleur-Niekraszewicz, L.A., Dias, J.F., Alves, M.C., Silveira, P.C.L., Nesi, R.T., Carvalho, F., Zocche, J.J., Pinho, R.A., 2020. Pulmonary oxidative stress in wild bats exposed to coal dust: a model to evaluate the impact of coal mining on health. Ecotoxicol. Environ. Saf. 191. https://doi.org/10.1016/j.ecoenv.2020.110211.
Pietrogrande, M.C., Bertoli, I., Clauser, G., Dalpiaz, C., Dell'Anna, R., Lazzeri, P., Lenzi, W., Russo, M., 2021. Chemical composition and oxidative potential of atmospheric particles heavily impacted by residential wood burning in the Alpine region of Northern Italy. Atmos. Environ., 118360 https://doi.org/10.1016/j.atmosenv.2021.118360.
Qiao, H., Chen, S., Dong, X., Dong, K., 2019. Has China's coal consumption actually reached its peak? National and regional analysis considering cross-sectional dependence and heterogeneity. Energy Econ. 84, 104509. https://doi.org/10.1016/j.eneco.2019.104509.
Qin, S., Zhao, C., Li, Y., Zhang, Y., 2015. Review of coal as a promising source of lithium. Int. J. Oil, Gas Coal Technol. https://doi.org/10.1504/IJOGCT.2015.067490.
Querol, X., Fernandez Turiel, J.L., Lopez Soler, A., Duran, M.E., 1992. Trace elements in high-S subbituminous coals from the Teruel Mining District, northeast Spain. Appl. Geochem. 7, 547–561. https://doi.org/10.1016/0883-2927(92)90070-J.
Querol, X., Whateley, M.K.G., Fernández-Turiel, J.L., Tuncali, E., 1997. Geological controls on the mineralogy and geochemistry of the Beypazari lignite, central Anatolia, Turkey. Int. J. Coal Geol. 33, 255–271. https://doi.org/10.1016/S0166-5162(96)00044-4.
Querol, X., Zhuang, X., Font, O., Izquierdo, M., Alastuey, A., Castro, I., van Drooge, B.L., Moreno, T., Grimalt, J.O., Elvira, J., Cabañas, M., Bartroli, R., Hower, J.C., Ayora, C., Plana, F., López-Soler, A., 2011. Influence of soil cover on reducing the environmental impact of spontaneous coal combustion in coal waste gobs: a review and new experimental data. Int. J. Coal Geol. 85, 2–22. https://doi.org/10.1016/j.coal.2010.09.002.
Rahman, I., Adcock, I.M., 2006. Oxidative stress and redox regulation of lung inflammation in COPD. Eur. Respir. J. 28, 219–242. https://doi.org/10.1183/09031936.06.00053805.
Ren, Q., Zhang, Y., Arauzo, I., Shan, L., Xu, J., Wang, Y., Su, S., Hu, S., Xiang, J., 2021. Roles of moisture and cyclic loading in microstructures and their effects on mechanical properties for typical chinese bituminous coals. Fuel 293, 120408. https://doi.org/10.1016/j.fuel.2021.120408.
Sánchez Jiménez, A., Van Tongeren, M., Cherrie, J.W., 2011. A Review of Monitoring Methods for Inhalable Hardwood Dust. Inst. Occup. Med P937/1A.
Schins, R.P.F., Borm, P.J.A., 1999. Mechanisms and mediators in coal dust induced toxicity: a review. Ann. Occup. Hyg. 43, 7–33. https://doi.org/10.1016/S0003-4878(98)00069-6.

Shi, X., Dalal, N.S., 1992. The role of superoxide radical in chromium(VI)-generated hydroxyl radical: the Cr(VI) haber-weiss cycle. Arch. Biochem. Biophys. 292, 323–327. https://doi.org/10.1016/0003-9861(92)90085-B.
Shi, X., Dalal, N.S., Kasprzak, K.S., 1992. Generation of free radicals from lipid hydroperoxides by Ni2 in the presence of oligopeptides. Arch. Biochem. Biophys. 299, 154–162. https://doi.org/10.1016/0003-9861(92)90257-W.
Shimura, K., Matsuo, A., 2019. Using an extended CFD-DEM for the two-dimensional simulation of shock-induced layered coal-dust combustion in a narrow channel. Proc. Combust. Inst. 37, 3677–3684. https://doi.org/10.1016/j.proci.2018.07.066.
Soltani, N., Keshavarzi, B., Sorooshian, A., Moore, F., Dunster, C., Dominguez, A.O., Kelly, F.J., Dhakal, P., Ahmadi, M.R., Asadi, S., 2018. Oxidative potential (OP) and mineralogy of iron ore particulate matter at the Gol-E-Gohar Mining and Industrial Facility (Iran). Environ. Geochem. Health 40, 1785–1802. https://doi.org/10.1007/s10653-017-9926-5.
Stach, E., Mackowsky, M.-T., Teichmüller, M., Taylor, G.H., Chandra, D., Teichmüller, R., 1982. Stach's Textbook of Coal Petrology. Gebrüder Borntraeger Berlin Stuttgart, p. 535.
Stohs, S.J., Bagchi, D., 1995. Oxidative mechanisms in the toxicity of metal ions. Free Radic. Biol. Med. 18, 321–336. https://doi.org/10.1016/0891-5849(94)00159-H.
Strlič, M., Kolar, J., Šelih, V.S., Kocar, D., Pihlar, B., 2003. A comparative study of several transition metals in fenton-like reaction systems at circum-neutral pH. Acta Chim. Slov. 50, 619–632.
Swaine, D.J., 1990. Trace Elements in Coal. Butterworth.
Tang, Z., Chai, M., Cheng, J., Jin, J., Yang, Y., Nie, Z., Huang, Q., Li, Y., 2017. Contamination and health risks of heavy metals in street dust from a coal-mining city in eastern China. Ecotoxicol. Environ. Saf. 138, 83–91. https://doi.org/10.1016/j.ecoenv.2016.11.003.
Tian, H.Z., Lu, L., Hao, J.M., Gao, J.J., Cheng, K., Liu, K.Y., Qiu, P.P., Zhu, C.Y., 2013. A review of key hazardous trace elements in Chinese coals: abundance, occurrence, behavior during coal combustion and their environmental impacts. Energy Fuel 27, 601–614. https://doi.org/10.1021/ef3017305.
Trechera, P., Moreno, T., Córdoba, P., Moreno, N., Zhuang, X., Li, B., Li, J., Shangguan, Y., Kandler, K., Dominguez, A.O., Kelly, F., Querol, X., 2020. Mineralogy, geochemistry and toxicity of size-segregated respirable deposited dust in underground coal mines. J. Hazard. Mater. 399, 122935. https://doi.org/10.1016/j.jhazmat.2020.122935.
Trechera, P., Moreno, T., Córdoba, P., Moreno, N., Zhuang, X., Li, B., Li, J., Shangguan, Y., Dominguez, A.O., Kelly, F., Querol, X., 2021. Comprehensive evaluation of potential coal mine dust emissions in an open-pit coal mine in Northwest China. Int. J. Coal Geol. 235, 103677. https://doi.org/10.1016/j.coal.2021.103677.
Valko, M., Morris, H., Cronin, M.T.D., 2005. Metals, toxicity and oxidative stress. Curr. Med. Chem. 12, 1161–1208.
Wang, H., Dlugogorski, B.Z., Kennedy, E.M., 2003. Coal oxidation at low temperatures: oxygen consumption, oxidation products, reaction mechanism and kinetic modelling. Prog. Energy Combust. Sci. https://doi.org/10.1016/S0360-1285(03)00042-X.
Wang, Y., Gu, A., Zhang, A., 2011. Recent development of energy supply and demand in China, and energy sector prospects through 2030. Energy Policy 39, 6745–6759. https://doi.org/10.1016/j.enpol.2010.07.002.
Wang, H., Du, M.L., Zhang, G.T., 2014. Concentration and distribution of Cr, Pb and Zn in the Jurassic coals from northern Shaanxi and Ningxia, China. Adv. Mater. Res. 989–994, 1415–1418. https://doi.org/10.4028/www.scientific.net/AMR.989-994.1415.
Wang, P., Ji, D., Yang, Y., Zhao, L., 2016. Mineralogical compositions of Late Permian coals from the Yueliangtian mine, western Guizhou, China: comparison to coals from eastern Yunnan, with an emphasis on the origin of the minerals. Fuel 181, 859–869. https://doi.org/10.1016/j.fuel.2016.05.043.
Wang, H., Zhang, L., Wang, D., He, X., 2017. Experimental investigation on the wettability of respirable coal dust based on infrared spectroscopy and contact angle analysis. Adv. Powder Technol. 28, 3130–3139. https://doi.org/10.1016/j.apt.2017.09.018.
WCA, 2020. World Coal Association [WWW Document]. https://www.worldcoal.org/.
Weber, R.J., Guo, H., Russell, A.G., Nenes, A., 2016. High aerosol acidity despite declining atmospheric sulfate concentrations over the past 15 years. Nat. Geosci. 9, 282–285. https://doi.org/10.1038/ngeo2665.
Wei, W., Mushtaq, Z., Sharif, M., Zeng, X., Wan-Li, Z., Qaisrani, M.A., 2020. Evaluating the coal rebound effect in energy intensive industries of China. Energy 207, 118247. https://doi.org/10.1016/j.energy.2020.118247.
WHO, 2000. WHO Air Quality Guidelines [WWW Document]. Second ed. WHO Reg. Off. Eur. Copenhagen, Denmark.
Wilhelm Filho, D., Júnior, S.Á., Possamai, F.P., Parisotto, E.B., Moratelli, A.M., Garlet, T.R., Inácio, D.B., Torres, M.A., Colepicolo, P., Dal-Pizzol, F., 2010. Antioxidant therapy attenuates oxidative stress in the blood of subjects exposed to occupational airborne contamination from coal mining extraction and incineration of hospital residues. Ecotoxicology 19, 1193–1200. https://doi.org/10.1007/s10646-010-0503-2.
Xu, C., Wang, D., Wang, H., Xin, H., Ma, L., Zhu, X., Zhang, Y., Wang, Q., 2017. Effects of chemical properties of coal dust on its wettability. Powder Technol. 318, 33–39. https://doi.org/10.1016/j.powtec.2017.05.028.
Yang, A., Jedynska, A., Hellack, B., Kooter, I., Hoek, G., Brunekreef, B., Kuhlbusch, T.A.J., Cassee, F.R., Janssen, N.A.H., 2014. Measurement of the oxidative potential of PM2.5 and its constituents: the effect of extraction solvent and filter type. Atmos. Environ. 83, 35–42. https://doi.org/10.1016/j.atmosenv.2013.10.049.
Yang, J., Wu, Jingli, He, T., Li, L., Han, D., Wang, Z., Wu, Jinhu, 2016. Energy gases and related carbon emissions in China. Resour. Conserv. Recycl. 113, 140–148. https://doi.org/10.1016/j.resconrec.2016.06.016.
Yu, H., Wei, J., Cheng, Y., Subedi, K., Verma, V., 2018. Synergistic and antagonistic interactions among the particulate matter components in generating reactive oxygen species based on the dithiothreitol assay. Environ. Sci. Technol. 52, 2261–2270. https://doi.org/10.1021/acs.est.7b04261.
Yu, H., Gao, Y., Zhou, R., 2020. Oxidative stress from exposure to the underground space environment. Front. Public Health https://doi.org/10.3389/fpubh.2020.579634.
Yuan, J., 2018. The future of coal in China. Resour. Conserv. Recycl. https://doi.org/10.1016/j.resconrec.2016.12.006.
Yuzhuang, S., Cunliang, Z., Yanheng, L., Jinxi, W., 2015. Anomalous concentrations of rare metal elements, rare-scattered (dispersed) elements and rare earth elements in the coal from Iqe Coalfield, Qinghai Province, China. Acta Geol. Sin. Engl. Ed. 89, 229–241. https://doi.org/10.1111/1755-6724.12407.
Zazouli, M.A., Dehbandi, R., Mohammadyan, M., Aarabi, M., Dominguez, A.O., Kelly, F.J., Khodabakhshloo, N., Rahman, M.M., Naidu, R., 2021. Physico-chemical properties and reactive oxygen species generation by respirable coal dust: implication for human health risk assessment. J. Hazard. Mater. 405, 124185. https://doi.org/10.1016/j.jhazmat.2020.124185.
Zhang, W., Rezaee, M., Bhagavatula, A., Li, Y., Groppo, J., Honaker, R., 2015. A review of the occurrence and promising recovery methods of rare earth elements from coal and coal by-products. Int. J. Coal Prep. Util. 35, 295–330. https://doi.org/10.1080/19392699.2015.1033097.
Zhang, W., Noble, A., Yang, X., Honaker, R., 2020. Lithium leaching recovery and mechanisms from density fractions of an Illinois Basin bituminous coal. Fuel 268, 117319. https://doi.org/10.1016/j.fuel.2020.117319.
Zhang, R., Liu, S., Zheng, S., 2021. Characterization of nano-to-micron sized respirable coal dust: particle surface alteration and the health impact. J. Hazard. Mater. 413, 125447. https://doi.org/10.1016/j.jhazmat.2021.125447.
Zhang, Y.J., Huang, C., Lv, Y.S., Ma, S.X., Guo, Y., Zeng, E.Y., 2021. Polycyclic aromatic hydrocarbon exposure, oxidative potential in dust, and their relationships to oxidative stress in human body: a case study in the indoor environment of Guangzhou, South China. Environ. Int. 149, 106405. https://doi.org/10.1016/j.envint.2021.106405.
Zhuang, X., Querol, X., Alastuey, A., Juan, R., Plana, F., Lopez-Soler, A., Du, G., Martynov, V.V., 2006. Geochemistry and mineralogy of the Cretaceous Wulantuga high-germanium coal deposit in Shengli coal field, Inner Mongolia, Northeastern China. Int. J. Coal Geol. 66, 119–136. https://doi.org/10.1016/j.coal.2005.06.005.
Zhuang, X., Su, S., Xiao, M., Li, J., Alastuey, A., Querol, X., 2012. Mineralogy and geochemistry of the Late Permian coals in the Huayingshan coal-bearing area, Sichuan Province, China. Int. J. Coal Geol. 94, 271–282. https://doi.org/10.1016/j.coal.2012.01.002.
Zosky, G.R., Bennett, E.J., Pavez, M., Beamish, B.B., 2021. No association between pyrite content and lung cell responses to coal particles. Sci. Rep. 11, 8193. https://doi.org/10.1038/s41598-021-87517-z.